Mobilization of poly- and perfluoroalkyl substances (PFAS) from heterogeneous soils: Desorption by ethanol/xanthan gum mixture

Ali Batikh, Stéfan Colombano, Maxime Cochennec, Dorian Davarzani, Arnault Perrault, Julie Lions, Julien Grandclément, Dominique Guyonnet, Anne Togola, Clément Zornig, et al.

Journal of Hazardous Materials 481 (2025) 136496

Contents lists available at ScienceDirect

Journal of Hazardous Materials

journal homepage: www.elsevier.com/locate/jhazmat

Mobilization of poly- and perfluoroalkyl substances (PFAS) from heterogeneous soils: Desorption by ethanol/xanthan gum mixture

Ali Batikh [a,b,c,*], Stéfan Colombano [a], Maxime Cochennec [a], Dorian Davarzani [a], Arnault Perrault [c], Julie Lions [a], Julien Grandclément [c], Dominique Guyonnet [a], Anne Togola [a], Clément Zornig [a], Nicolas Devau [a], Fabien Lion [a], Amir Alamooti [a], Sébastien Bristeau [a], Mohamed Djemil [a], Eric D. van Hullebusch [b]

[a] BRGM (French Geological Survey), 3 Avenue Claude Guillemin, Orléans 45100, France
[b] Université Paris Cité, Institut de physique du globe de Paris, CNRS, F-75005 Paris, France
[c] COLAS Environnement, 91, rue de la Folliouse, 01700 Miribel, France

HIGHLIGHTS

- Ethanol (50 % v/v) did not impact the shear-thinning behavior of xanthan gum solutions.
- A positive correlation was observed between PFAS sorption and octanol-water coefficient.
- Overshoot in PFAS concentrations was observed after flushing with ethanol (50 % v/v) and xanthan-ethanol mixture (in 1D column experiments).
- More than 93 % of different PFASs were recovered after flushing by xanthan-ethanol mixture.
- Numerical modeling successfully reproduces breakthrough curves.

GRAPHICAL ABSTRACT

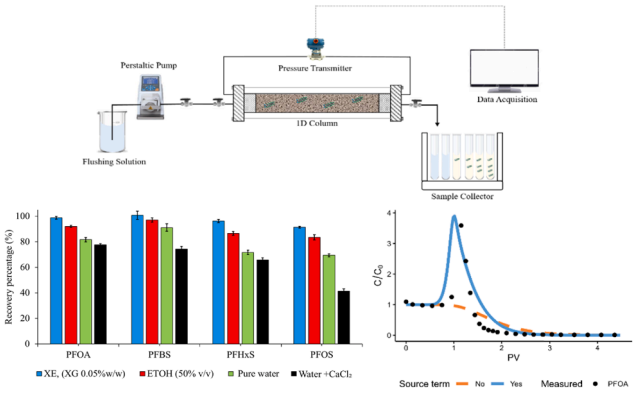

ARTICLE INFO

Keywords:
Poly- and perfluoroalkyl substances (PFAS)
Non-Newtonian fluids (NNF)
Desorption
Alcohol
Heterogeneity of porous media

ABSTRACT

Remediating soils contaminated by per- and polyfluoroalkyl substances (PFAS) is a challenging task due to the unique properties of these compounds, such as variable solubility and resistance to degradation. In-situ soil flushing with solvents has been considered as a remediation technique for PFAS-contaminated soils. The use of non-Newtonian fluids, displaying variable viscosity depending on the applied shear rate, can offer certain advantages in improving the efficiency of the process, particularly in heterogeneous porous media. In this work, the efficacy of ethanol/xanthan mixture (XE) in the recovery of a mixture of perfluorooctane sulfonate (PFOS), perfluorooctanoic acid (PFOA), perfluorohexane sulfonate (PFHxS), and perfluorobutane sulfonate (PFBS) from soil has been tested at lab-scale. XE's non-Newtonian behavior was examined through rheological measurements, confirming that ethanol did not affect xanthan gum's (XG) shear-thinning behavior. The recovery of PFAS in batch-desorption exceeded 95 % in ethanol, and 99 % in XE, except for PFBS which reached 94 %. 1D-column

* Corresponding author at: BRGM (French Geological Survey), 3 Avenue Claude Guillemin, Orléans 45100, France.
E-mail addresses: a.batikh@brgm.fr, aly.batikh@gmail.com (A. Batikh).

https://doi.org/10.1016/j.jhazmat.2024.136496
Received 8 January 2024; Received in revised form 3 November 2024; Accepted 11 November 2024
Available online 17 November 2024

experiments revealed overshoots in PFAS breakthrough curves during ethanol and XE injection, due to over-solubilization. XE, (XG 0.05 % w/w) could recover 99 % PFOA, 98 % PFBS, 97 % PFHxS, and 92 % PFOS. Numerical modeling successfully reproduces breakthrough curves for PFOA, PFHxS, and PFBS with the convection-dispersion-sorption equation and Langmuir sorption isotherm.

1. Introduction

Per- and polyfluoroalkyl (PFAS) substances have recently attracted a lot of attention because of their ubiquitous presence in the environment and potential effects on human health [1,2]. PFAS are widely present in the air, water, and soil as a result of their widespread use in a variety of industrial and consumer items, such as water-resistant textiles, aqueous fire-fighting foam (AFFF), and non-stick cookware [3]. Their fluor-carbon bounds provide them exceptional chemical and thermal resistance, as well as a highly stable nature in the environment [4,5]. PFAS are characterized by their environmental persistence which has led to the label “Forever chemicals”. Concerns regarding the long-term impacts of PFAS exposure on human health and ecosystems have been raised due to their persistence and bio-accumulative nature [6,7].

In the current decade, concentrations of various PFAS have been determined in groundwater in the range of < 0.03 ng.L^{-1} to 6.75 mg.L^{-1} for perfluorooctanoic acid (PFOA), 0.01 ng.L^{-1} to 4.6 mg.L^{-1} for perfluorooctane sulfonate (PFOS), 0.01 ng.L^{-1} to 2.38 mg.L^{-1} for perfluorohexane sulfonate (PFHxS), and 0.01 ng.L^{-1} to 0.822 mg.L^{-1} for perfluorobutane sulfonate (PFBS) [8], in surface water system, reaching levels of up to 100 ng.L^{-1} [9] and in drinking water, exceeding. 500 ng.L^{-1} (Dixit et al., 2021). These concentrations exceed the drinking water threshold set by the U.S. Environmental Protection Agency 4 ng.L^{-1} for PFOS and PFOA and 10 ng.L^{-1} for PFHxS [10], and those set by the Europe Union 100 ng.L^{-1} for the sum of 20 PFAS (including PFOA and PFOS) and 500 ng.L^{-1} for all total PFAS [11], posing substantial health risks to humans, including renal toxicity, hepatotoxicity, and carcinogenicity [12,13].

Soil has been identified as a prominent and persistent source of PFAS pollution at contaminated sites [14]. The occurrence of soil and sediments contaminated by PFAS results from various sources, such as the use of bio-solids in agriculture (soil amendments) [15], leachates from landfills [16], discharges from fluoropolymer manufacturing plants [17], and notably, the widespread use of aqueous fire-fighting foam (AFFF) in military sites and airports [18,19]. Global soil PFAS concentrations have been reported in the range of tens of ng.g^{-1} by several studies in China, the United States, Korea, Norway, and Belgium [20-22]. Brusseau et al. [23] revealed that soils in numerous military installations in the USA contained significant concentrations of PFOA at 50,000 ng.g^{-1} and PFOS at 373,000 ng.g^{-1}. In France, for instance, perfluorinated carboxylic acids (PFCA) were found in soil sampled from a fluoro-telomere production site at concentrations of 655 ng.g^{-1} [24], while firefighter training sites had a maximum of different PFAS compounds (mainly PFOS) of 357.46 ng.g^{-1}, according to Dauchy et al. [25]. These values highlight the wide range of PFAS contamination and its possible global environmental impact. Considering the rising concentrations of PFAS in soils and the associated risks to ecosystems and human health due to potential exposure through groundwater, there is a critical need to develop effective technology for the recovery of PFAS from soil and groundwater systems.

Remediation of PFAS-contaminated soils represents a challenging task due to the unique chemical properties of these substances [26]. Several remediation technologies have been tested for the remediation of PFAS including ex-situ methods such as bioremediation technology [27], oxidation/reduction processes [28,29], thermal processes [5], soil vitrification [30] and soil washing method using an in-situ approach [31] and an ex-situ one [32]. However, these methods showed various limitations and challenges such as high cost due to excavation, transportation, and energy requirements [33,34]. Compared to the previously mentioned remediation technologies, the in-situ soil flushing method has become a reliable and efficient method for the remediation of soil that has been contaminated by organic pollutants such as Polychlorinated biphenyl (PCB), Polycyclic Aromatic Hydrocarbons (PAHs), and different chlorinated hydrocarbons. This remediation technology has several advantages including the remediation of a large contaminated zone with minimized excavation and transport, negligible disturbance of soil structure, a small requirement of area for the equipment, and applications in both the saturated and the unsaturated zones [35]. Different additives can be injected into the soil, such as organic polymers [36] and co-solvents [37].

Solvents such as alcohol have been used for decades as a flushing solution for mobilizing and solubilizing different organic contaminants [38,39]. To date, solvents such as methanol, ethanol, and propanol have been used in the regeneration of various sorbents contaminated with PFAS. This application has been investigated in both batch and column PFAS regeneration studies involving granular and powdered activated carbon (GAC, PAC, respectively) as well as resin [40-42]. For batch-scale investigations, ethanol 50% volume fraction (v/v) has been consistently confirmed to be the best removal and regenerator solvent for PFAS, in particular PFOS and PFOA, from soils and sorbent materials [43,44]. This choice stems from its demonstrated advantages, including lower toxicity than methanol [45] and superior efficiency than propanol [35]. Moreover, column-scale studies have expanded on this by simulating more realistic conditions, where removal solutions flow through the porous medium (soil, sorbent materials). Siriwardena et al. [46] conducted a study on the efficacy of ethanol in regenerating a GAC column, revealing a removal efficiency of 64% for PFOS and 93% for PFOA. Senevirathna et al. [35] carried out experiments in columns. They reported removal of 98% for PFOS after injection of five bed-volumes of ethanol (50% v/v). Shaikh et al. [47] found comparable outcomes, ethanol (50% v/v) achieved a remarkable 89% regeneration of PFOA from the activated carbon column after injection of eight bed-volumes.

Despite ethanol’s advantage over PFAS recovery, heterogeneous permeability in subsurface soil may pose challenges in uniformly distributing removal solutions during in-situ soil flushing. This is due to the formation of preferential pathways, resulting in significant non-swept areas within low-permeability layers. Additionally, the permeability could be reduced resulting from the reduction of soil porosity due to the sorption of PFAS to soil particles, which could decrease the effectiveness and reliability of soil flushing [35]. The use of non-Newtonian fluid (bio-polymer solution) can present advantages for improving the homogeneity of the injection of additives in heterogeneous soils. The most recent improvements in in-situ soil flushing technologies involve the injection of non-Newtonian fluids such as polymer (xanthan gum, guar gum) [48,49] and foam [50,51]. The shear thinning behavior of polymers improves the mobility of flushing solution and the sweeping in porous media especially in lower permeability zones [52]. According to Gauthier and Kueper [53], a flushing solution consisting of xanthan gum and two distinct alcohols (ethanol and n-propanol) was able to remove 94% of PolyChloroBiphenyls from sand in a 2D tank system. Other studies, demonstrated that xanthan gum could improve the sweeping efficiency in heterogeneous sandbox experiments [54].

In addition, the experimental data are used to calibrate a numerical model for sorbed solute transport in soil columns. Several models have been proposed and tested in the literature [55,56]. Most of them focus on the transport of diluted PFAS in groundwater/soil, either under water-saturated or unsaturated [57], vadose zone conditions. For

saturated soils, the options include (1) a convection-dispersion equation with an additional equilibrium non-linear term for adsorption (e.g., Langmuir isotherm, or a lumped term to include different sorption phenomena), [58], (2) modification of the convection-dispersion equation to include two adsorption sites (one instantaneous and one is rate-limited), namely the two-site model (TSM) [59-61] and (3) more complex models that can reproduce anomalous transport (deviating from Fick's diffusion) due to, for example, soil heterogeneity, rate-limited solid adsorption, etc. [62,63]. While the literature indicates that the two-site model is the most commonly used, it appears that the observation of non-equilibrium sorption phenomena during 1D transport of PFAS in sand columns is mostly observed for PFOS, while the breakthrough curves for PFOA and PFHxS, for example, are often compatible with equilibrium (non-linear) sorption model [60]. On the other hand, to the best of our knowledge, no work has yet applied any of the above models to reproduce desorption experiments using a fluid other than the one used during contamination, whereas this situation mimics a widely used family of remediation technology, as discussed above.

The objective of this study is to evaluate the effectiveness of the polymer-alcohol mixture in removing four PFAS including PFOS, PFOA, PFHxS, and PFBS from contaminated soil. The first phase involved assessing the rheological behavior of the xanthan-ethanol mixture at various concentrations of polymer in the bulk. Subsequently, a series of batch sorption and desorption experiments were conducted to understand the sorption behavior of these compounds as well as the efficiency of ethanol with and without xanthan gum on the recovery of PFAS. In addition to these experiments, a series of 1D porous column experiments were conducted to assess the efficacy of the introduced polymer in ethanol solutions for PFAS recovery. Additionally, the simulation part of this work is to compare the experimental data with the convection-dispersion-sorption model, using an equilibrium, non-linear, approach for sorption, applied to adsorption and desorption with the background solution free of PFAS and other fluids (polymer, ethanol). Considering the paucity of investigations regarding the efficiency of non-Newtonian fluids as mixture partners for the recovery of PFAS-contaminated soil, our study proposes an analysis of the potential benefits of combining a solubilizing agent and a non-Newtonian agent.

2. Materials and methods

2.1. Materials

Four PFAS representatives including, PFOS (CAS# 1763–23-1, Sigma Aldrich, 99.8% purity), PFBS (CAS# 375–73-5, Sigma Aldrich, 99.8% purity), PFHxS (CAS# 3871–99-6, Sigma Aldrich, 99.9% purity) and PFOA (CAS# 335–67-1, Sigma Aldrich, 99% purity) were used in sorption and desorption experiments. Ultrapure water was used from the Milli-Q purification system. Different solvents for chromatography including water, ammonium acetate, and glacial acetic acid (Reagent-Plus grade ≥99%) were supplied by Sigma-Aldrich. Calcium chloride ($CaCl_2$) for enhancing the ionic strength of the PFAS solution was provided by Acros Organics. Ethanol (99%), and high-performance liquid chromatography (HPLC) grade methanol were obtained from Fischer Scientific. Bio-polymer xanthan gum was provided by Sigma-Aldrich.

2.2. Methods

2.2.1. Soil preparation

The soil or porous media used in this study was man-made soil, which contains 92% quartz sand, 5% mineral clay, and 3% organic matter. The soil pH was measured in $CaCl_2$ supernatants using a VWR pH meter (pH 1100 H). The supernatant was collected from a suspension of soil (soil/solution = 1/5) in 0.01 mol.L^{-1} of $CaCl_2$ solution according to ISO protocol (ISO 10390:2021) (Table 1). The soil was mixed manually by hand, using the quartering method, for approximately 4 h for all the experiments presented in this study. The sand was initially sieved to achieve a particle size of 0.8–1.25 mm and rinsed to eliminate any debris. The clay consisted of various minerals including 12.9% smectite, 10.4% illite, 7.2% goethite, and predominantly 45.4% kaolinite. Organic matter sourced from compost was used for several advantages such as high organic content, accessibility, and cost-effectiveness The Total Organic Carbon (TOC) in the soil was measured using the TOC Shimadzu device. The TOC in the man-made soil is 1.14%, given a bulk density of 1.6 g.cm^{-3}. The clay and organic matter were crushed and sieved to a particle size smaller than 1.25 mm before mixing with the sand. This man-made soil ensures a homogeneous distribution of organic matter and clay in the blend. In order to maintain homogeneity, the soil was first prepared by thoroughly mixing sand and clay. After that, organic matter was progressively added and mixed until the soil was completely covered. Water was added gradually while mixing in order to achieve a constant texture and moisture content. This reconstituted soil is representative of classic French alluvial soils [64,65].

2.2.2. Rheological behavior of polymer-ethanol solutions

Xanthan gum was selected based on various factors, such as biodegradability, non-Newtonian behavior, ecological compatibility, and market accessibility. The polymer solution was acquired by dissolving a specified quantity of xanthan gum powder in purified water under gentle agitation using a top-mounted stirrer (IKA RW14) at 250–400 rpm for 3 h. Ethanol (ETOH) was prepared by diluting alcohol in water for the corresponding ratio (1:1). Xanthan/ethanol mixture (XE) was prepared by introducing ETOH (50% v/v) to xanthan gum solution while gently stirring to prevent ethanol from evaporating.

The rheological behavior of all solutions prepared was analyzed using a controlled rheometer Haake Mars 60 Thermo Fisher (equipped with cone-plate geometry) in order to understand the effect of ethanol on the non-Newtonian behavior of xanthan gum. Each concentration of xanthan gum solution with and without ethanol was examined in triplicate. The shear rate was measured over time with the specified force. The applied shear stress ranged from 0.01 to 100 s^{-1}.

2.2.3. Batch sorption and desorption experiments

All batch experiments were carried out in 50 mL polypropylene (PP) centrifuge tubes. A mixture of PFAS solution was used during each experiment. The concentration of each substance was equal to 5 mg.L^{-1}. The PFAS concentration chosen represents the average concentration of PFOS and PFOA in the groundwater of different sites such as fire-training areas and manufacturing plants [8]. This concentration was achieved by diluting each PFAS stock solution in a volume of Milli-Q water containing $CaCl_2$ at 10 mM. The concentration of $CaCl_2$ was chosen to enhance the sorption rate of PFAS onto the soil [66]. Sorption tubes, each containing 11.25 g of soil to 25 mL of PFAS solution (L/S = 2.22) were prepared in triplicate. The tubes were subsequently mixed horizontally in an orbital shaker to optimize the interaction between the soil and the PFAS solution at different time intervals (0.5 h, 2 h, 6 h, and 24 h) at a speed of 160 rpm while maintaining a temperature of 22 °C. The suspension was periodically centrifuged at 10000 rpm for 10 min. Following that, an aliquot of the supernatant was collected and analyzed by Liquid chromatography-tandem-mass spectrometry (LC-MS/MS).

Table 1
Physical and chemical properties of the soil used in the experiments.

Soil	Sand (%)	Clay (%)	Organic matter (%)	Soil pH	TOC (%)	Permeability k (m^2)	Porosity (%)	Pore volume PV (mL)
Sandy soil	92	5	3	6.5	1.14	93.10^{-12}	39	150

For the desorption experiments, the residual wet soil from sorption tests was utilized. PFAS-free solutions consisting of ethanol (50% v/v) with and without xanthan gum at several concentrations (0.5, 1 and 2 g.L^{-1}) were introduced to the wet soil using the same L/S ratio as in the sorption test. Subsequently, the suspensions were mixed, centrifuged, and analyzed using the same procedure as that used for sorption.

2.2.4. Column experiments

A sequence of 1D column experiments was conducted to determine the sorption of the investigated PFAS onto the soil and the desorption rate for the flushing solutions. The visual representation of the experimental setup used for the 1D column experiment is presented in Fig. 1. We used a borosilicate glass column with dimensions of 4 cm inner diameter (ID) × 30 cm (length). Two metallic grids (mesh) with a pore size of 150 µm were installed on both sides of the column to hold the soil. Pharmed BPT tubes were used to limit PFAS sorption. The influent of the column was connected to an Ismatec Reglo ICC digital peristaltic pump with four channels. An Emerson differential pressure transducer was connected to both ends of the column to gauge the pressure variation during the experiments. A mass balance was placed under the injected solution to verify the mass of the influent.

The columns were filled vertically with soil in 2 cm layers, and the boundary between accretions was delicately mixed with a spatula to reduce stratification. Once the packing was completed, a leak test was conducted to verify the column's airtightness by introducing 1 bar of gas pressure. Following this, the column underwent a 30-minute CO_2 flushing process to enhance water saturation, as CO_2 gas exhibits high solubility in water. Subsequently, four pore volumes (PV) of demineralized water were injected vertically upward into the column at a rate of 1 mL.min^{-1}. The column weight was measured both before and after the water saturation process to calculate the PV and porosity. After achieving full water saturation, the permeability test was conducted horizontally and was determined by measuring the pressure drop corresponding with several flow rates introduced according to Darcy's law. A nonreactive tracer experiment was conducted by introducing 5 PV of KBr (5 g.L^{-1}) to quantify the dispersivity and flow conditions of the porous media. Exhaust samples were collected by a sample collector in PP tubes at a volume of 25 mL. To examine the sorption behavior of all PFAS studied, 5 PV of an aqueous PFAS solution with a concentration of 5 mg.L^{-1} was injected in a vertical upward direction at a flow rate of 2 mL.min^{-1} to ensure a gravity-stable displacement. Once the sorption injection was finished, a flush injection was carried out by introducing horizontally 5 PV of PFAS-free solution. Effluent breakthrough curves for tracer and PFAS were graphed as the ratio of the relative concentration (C_0) to the initial concentration (C) as a function of the injected PV.

2.3. Analysis

2.3.1. Sample analysis

Water samples (20 mL) were collected in 50 mL PP tubes as a blank control (containing 20 mL of HPLC water). After any dilution with water, the samples were mixed with 50% of methanol, except for the experiment with xanthan gum for which a maximum of 30% of methanol can be used to avoid xanthan gum precipitation. 0.44 mL volume of the previous preparation is transferred to a PP vial/cap and spiked with acid acetic (5%) and 50 µL of the internal standard solution (2 µg.L^{-1} in methanol) and vortexed, resulting in a surrogate concentration of 200 ng.L^{-1} and 0.1% acid acetic in the diluted solution. Samples were analyzed by LC-MS/MS. To avoid cross-contamination, methanolic blanks are injected between high-concentration samples and water samples are analyzed to check that there is no contamination.

PFAS analyses were carried out using a Waters TQXS system coupled to a Waters UHPLC system equipped with an Acquity BEH C18 Column (1.7 µm particle size, 100 × 2.1 mm, Waters) heated at 35 °C and a delay C18 column (isolator column 50 × 2.1 mm, Waters) to avoid PFAS contamination from the chromatographic system. The injection volume was 10 µL and the mobile phase was a mixture of 2 mM Ammonium Acetate in H_2O (A) and 2 mM Ammonium Acetate in MEOH (B) at a 0.3 mL.min^{-1} flow. The gradient elution started with 95% A and gradually changed up to 95% B within 6.5 min. This ratio was kept for 0.5 min and then reversed into the initial conditions for 3 min. MS analysis was performed with the TQXS mass spectrometer, which operated in negative Electrospray Ionization mode (ESI). The source conditions were set as the following: desolvation temperature 500 °C, desolvation gas flow 1100 L.hr^{-1}, cone gas flow 150 L.hr^{-1}, capillary voltage −1000 V. The chromatograms were processed with the TargetLynx software. PFAS quantification was based on 9-point calibration curves (10 to 5000 ng.L^{-1}) having $R^2 > 0.99$ for all compounds. In these conditions, LQ was estimated to be 20 ng.L^{-1} (without consideration of sample dilution) regardless of the nature of the samples. Mass spectral parameters used for PFAS analysis are presented in Table S1 in supplementary materials.

2.3.2. Data analysis

2.3.2.1. Transport flow in porous media and modeling. The one-dimensional fluid flow in porous media is often described using Darcy velocity, U (m.s^{-1}), which can be expressed as follows [67]:

$$U = \frac{Q}{S} = \frac{K \quad \Delta P}{\mu L} \tag{1}$$

where Q ($m^3.s^{-1}$) is the flow rate, S (m^2) is the surface area of the porous media, K (m^2) is the permeability, ΔP (Pa) is the pressure drop, L (m) is

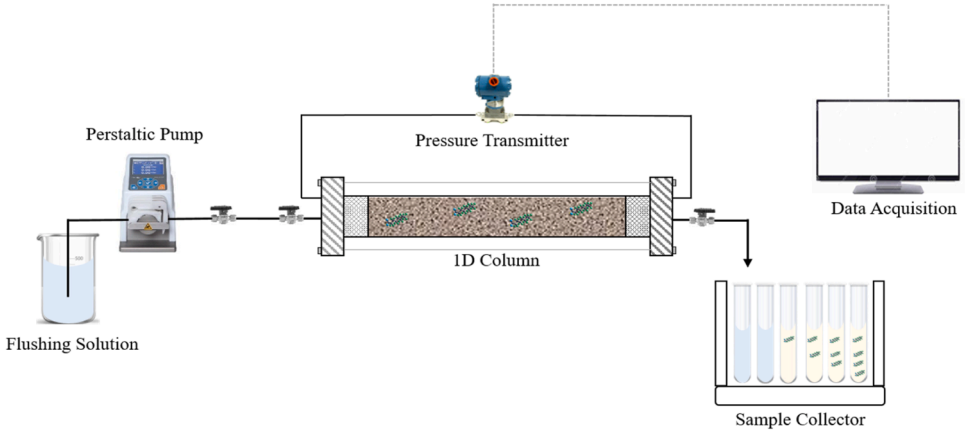

Fig. 1. Schematic representation of the experimental setups employed in this study.

the length of the porous media, and μ (Pa.s) is the dynamic viscosity.

For Newtonian fluid, the dynamic viscosity is the ratio of the shear stress τ (Pa) and the shear rate γ (s^{-1}):

$$\mu = \frac{\tau}{\gamma} \tag{2}$$

Regarding the modeling of the 1D column transport experiments, the convection/dispersion equation is used to obtain the longitudinal dispersivity, and the same equation is then used in combination with the Langmuir sorption isotherm to reproduce the PFAS transport in the saturated column, either for adsorption or desorption. The convection/dispersion/sorption equation reads [68]:

$$\phi \frac{\partial C}{\partial t} + \rho \frac{\partial C_s}{\partial t} + u \frac{\partial C}{\partial x} - D^* \frac{\partial^2 C}{\partial x^2} = 0 \tag{3}$$

where C is the PFAS concentration ($mol.m^{-3}$), ρ is the dry bulk density of the porous medium ($kg.m^{-3}$),

C_s is the concentration adsorbed to the solid ($mol.kg^{-1}$), $u = U/\phi$ is the linear average velocity ($m.s^{-1}$),

D^* is the hydrodynamic dispersion coefficient ($m^2.s^{-1}$). The Langmuir sorption isotherm implies that [69]:

$$C_s = \frac{C_{s,\max} \quad K_L C}{1 + K_L C} \tag{4}$$

where K_L is the Langmuir constant ($m^3.mol^{-1}$) and $C_{s,\max}$ is the sorption maximum ($mol.kg^{-1}$).

The convection/dispersion equation is then solved in COMSOL Multiphysics®, a finite element method-based software. The geometry is a 1D geometry of length 30 cm. The initial PFAS concentration is zero, and the inlet boundary condition is a constant concentration value based on the known concentration in the injected solution (Dirichlet condition). The outlet boundary condition is a flux-boundary condition involving each time step (Cauchy condition). For desorption, the same approach is used, but the inlet concentration is zero, and the initial concentration is the same as at the end of the adsorption tests. The values for K_L and $C_{s,\max}$ are found by solving a least-square minimization problem, for which the initial values are based on the literature, and the acceptable value range during optimization is more or less 100 times the initial value. The hydrodynamic dispersion coefficient was fitted based on the non-reactive tracer experiment.

2.3.2.2. Sorption and desorption batch parameters. The concentration of the PFAS compound sorbed in the soil after the sorption batch experiment C_s ($mg.g^{-1}$), is determined according to Eq. 5 [70]:

$$C_s = \frac{(C_{in} - C_w) \quad . \quad V}{m_{soil}} \tag{5}$$

where C_{in} ($mg.L^{-1}$) represents the initial PFAS concentration in the stock solution, C_w ($mg.L^{-1}$) represents the PFAS concentration obtained from liquid chromatography analysis, V (mL) is the volume of PFAS solution used in batch sorption, and m_{soil} (g) is the weight of dry soil.

Furthermore, the PFAS sorption percentage, S (%), was computed using the subsequent formula:

$$S(\%) = \frac{C_s . \quad m_{soil}}{C_{in} . \quad V} 100 \tag{6}$$

The desorption percentage D (%) was calculated by dividing the amount of PFAS removed by the one present in the soil used for the desorption batch experiment, according to the following equation:

$$D \quad (\%) = \frac{C_{w,des} \quad . \quad V}{C_{in,des} \quad . \quad m_{soil}} 100 \tag{7}$$

where, $C_{w,\ des}$ ($mg.L^{-1}$) is the concentration of PFAS after desorption analysis, and V (mL) and m_{soil} (g), are the volume of removal solution and the mass of dry soil used in desorption tests. $C_{in,\ des}$ ($mg.g^{-1}$) represents the initial concentration of PFAS in the residual soil from sorption tests. To better quantify this concentration, the amount of PFAS in residual water from the sorption test was taken into account following Eq. 8:

$$C_{in,des} = C_s + \frac{C_w . \quad V_{res}}{m_{soil}} \tag{8}$$

2.3.2.3. 1D column sorption and desorption parameters. The breakthrough curve explains the loading behavior of PFAS to be sorbed and desorbed from the soil. It is the plot of the relative concentration (C_0) to the initial concentration (C) as a function of the total pore volume injected (PV) [71]. The mass of PFAS sorbed ($m_{PFAS_{sorbed}}$; mg) on the soil is a function of the total flow rate (Q; $mL.min^{-1}$) injected and the area under sorption breakthrough curve (A) as expressed in the following equation:

$$m_{PFAS\ sorbed} = \frac{QA}{1000} \tag{9}$$

$$A = \int_{t=0}^{t=\ t_{total}} C_{effluent} dt \tag{10}$$

where $C_{effluent}$ ($mg.L^{-1}$) is the concentration of PFAS produced during the sorption process.

The mass of total PFAS injected is calculated via the equation:

$$m_{Total\ PFAS\ injected} = \frac{QC_0 \quad t_{total}}{1000} \tag{11}$$

where C_0 ($mg.L^{-1}$) is the inlet concentration of PFAS, and t_{total} (min) is the total time of PFAS injection.

The sorption yield (%) of PFAS in the soil is expressed as the following equation:

$$PFAS\ sorption(\%) = \frac{m_{PFAS\ sorbed}}{m_{Total\ PFAS\ injected}} 100 \tag{12}$$

The percent PFAS recovery is calculated according to the equation below:

$$PFAS\ removed(\%) = \frac{m_{PFAS\ effluent\ after\ desorption}}{m \quad _{PFAS\ sorbed}} 100 \tag{13}$$

3. Results and discussion

3.1. Rheological behavior of xanthan-ethanol mixture

Xanthan gum rheological behavior at different concentrations with and without ethanol was measured at ambient temperature. The steady shear viscosity as a function of different shear rates for the three concentrations of xanthan gum with and without ethanol 50% (v/v) is presented in Fig. 2. Experimental viscosity data was fitted by the Carreau model (Eq. 14) [72].

$$\frac{\mu - \mu_{\inf}}{\mu_0 - \mu_{\inf}} = \left[1 + (\lambda\gamma)^2\right]^{\frac{n-1}{2}} \tag{14}$$

where, zero and infinity shear rates viscosities (Pa.s) are denoted as μ_0 and μ_{inf}, λ (s) is the relaxation time, γ (s^{-1}) is the shear rate, and n (-) is the dimensionless power index. Carreau model fitting parameters are presented in Table S2 in supplementary materials. The fitting exceeds 98% confidence for xanthan gum Fig. 2 models due to its ability to accurately represent rheological behavior at very low shear rates [73,48,74].

According to the results represented in Fig. 2a, the steady shear viscosity of xanthan solutions increases while increasing the concentration. Experimental data indicates that doubling the concentration results in a noticeable decrease in the Newtonian region within the low

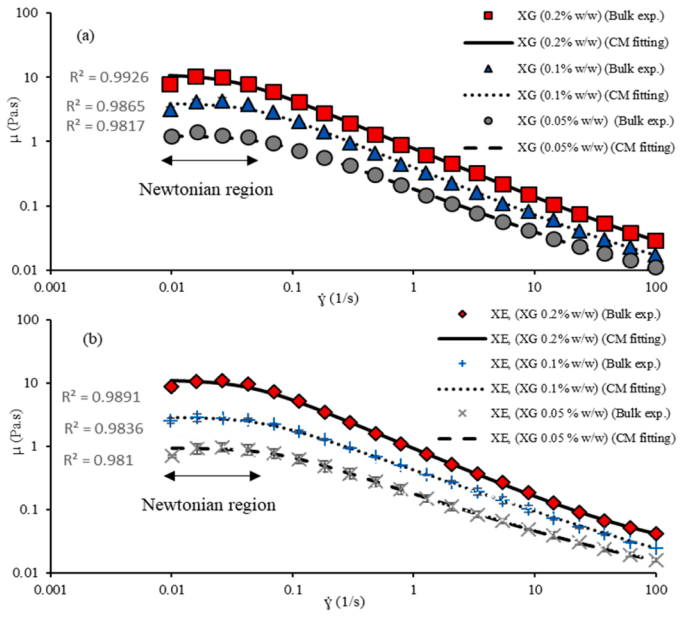

Fig. 2. Bulk viscosity of xanthan gum solution at different concentrations (0.5, 1, and 2 g.L^{-1}) without ethanol (a) and with ethanol (b) as a function of shear rate. Notes: CM = Carreau Model; XG = Xanthan Gum. Each data point and error bar are means and standard deviations of triplicates, respectively.

shear rates range (0.01–0.026 1/s). Additionally, a robust behavior of shear thinning was observed within the range of 0.05 to 100 (1/s), regardless of the polymer concentration being tested. This significant non-Newtonian behavior was caused by the alteration of the arrangement of the polymer chains in fragmented order at high shear rates region [73].

Fig. 2b, illustrates the influence of ethanol (50% v/v) on the rheological behavior of xanthan gum for different polymer concentrations. Three sets of measurements were conducted for every concentration of xanthan gum in the presence of ethanol (50% v/v) by extracting samples from the upper, middle, and lower sections of the mixture. Error bars are computed by finding the mean (average) of the data points and the standard deviation. The upper end of the error bar is positioned at the mean plus the standard deviation, while the lower end is positioned at the mean minus the standard deviation. For all concentrations of xanthan, a homogeneity was observed in the mixture with ethanol (50% v/v), which is consistent with the rheological measurements as well as observations reported by Flahive et al. [75].

As depicted in Fig. 2, the consistent shear thinning behavior was maintained for all concentrations of xanthan gum in the presence of ethanol (50% v/v). Furthermore, the addition of ethanol has not led to substantial changes in the rheological characteristics of xanthan gum.

Given that the addition of ethanol did not affect the non-Newtonian properties of the polymer, it follows that all of these mixtures examined in rheology will subsequently be examined in batch scale to determine whether the polymer as well as its concentration, impact the PFAS recovery by ethanol.

3.2. Sorption batch experiments

The percentage of PFOS, PFOA, PFHxS, and PFBS sorption from aqueous solution onto soil was examined in this study. Fig. 3 shows the sorption percentage of various PFAS at different contact time intervals (0–0.5 h, 0.5–2 h, 2–6 h, and 6–24 h). The samples were taken exactly at the specified time points (0.5 h, 2 h, 6 h, and 24 h). However, for clarity in presenting the sorption behavior over time, the results are shown as cumulative intervals (0–0.5 h, 0.5–2 h, 2–6 h, and 6–24 h). This approach allows for a clearer depiction of the sorption process over these

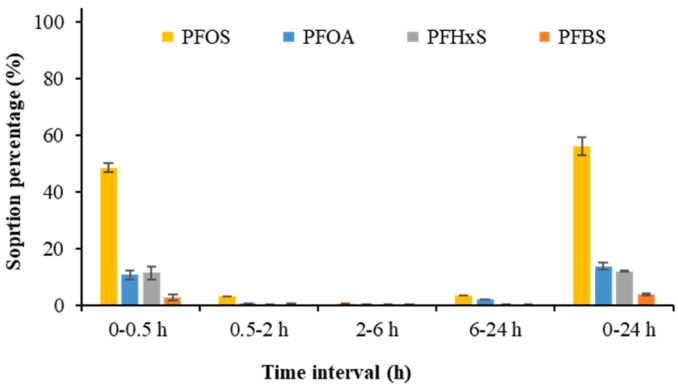

Fig. 3. Variation of sorption percentage versus time interval for different PFAS on the tested soil. The L/S ratio was 2.22 and the initial concentration of each PFAS was 5 mg.L^{-1}. Each data point and error bars are means and standard deviations of triplicates, respectively.

specific periods, highlighting any incremental changes in sorption within each interval.

One can see that each PFAS component exhibited its highest sorption percentage within the initial half hour (48.6% ± 1.5% for PFOS, 10.8% ± 1.6% for PFOA, 11.5% ± 2% for PFHxS, and 2.8% ± 0.8% for PFBS). It can be seen that the sorption equilibrium of PFHxS and PFBS was 2 h faster than PFOS and PFOA which required 24 h. Though the initial aqueous concentration of PFAS studied was the same (5 mg.L^{-1}), the equilibrium concentration of PFOS was the lowest one in comparison to other PFAS studied. For instance, the concentration of PFOS sorbed to soil was (4.83 ± 0.4 mg.kg^{-1}) much higher than PFOA (1.11 ± 0.1 mg.kg^{-1}), PFHxS (0.91 ± 0.2 mg.kg^{-1}) and PFBS (0.37 ± 0.1 mg.kg^{-1}) suggesting the strong affinity of PFOS to be sorbed onto soil than the other PFAS. These findings align with previous studies. Li et al. [76] tested the sorption of PFOS, PFOA, and PFBS on different soils with TOC ranging from 0.25 to 3.28%. They reported that the highest concentration of PFAS sorbed was 2.25 mg.kg^{-1} for PFOS, 1 mg.kg^{-1} for PFOA and 0.45 mg.kg^{-1} for PFBS. Furthermore, Chen et al. [66] studied the sorption of PFOA and PFOS onto various soil compositions and found that the equilibrium sorption time of PFAS was reached within 10–12 h. The distribution coefficient (K_d) values for PFAS varied with the length of the perfluorinated carbon chain [77]. Specifically, the K_d for PFOS, at 2.85 L.kg^{-1} was approximately 10 times greater than the K_d values for PFOA and PFHxS (0.32 and 0.27 L.kg^{-1}, respectively), and over 70 times higher than that of PFBS (0.05 L.kg^{-1}). These results align with previous research. Hubert et al. [78] reported K_d values of 2.51 and 0.44 L.kg^{-1} for PFOS and PFOA, respectively, in soils with grain size of 0.5 to 2 mm and organic content of almost 1.5%. Similarly, Oliver et al. [79] found comparable values for PFOA, PFOS, and PFHxS in soils with organic content ranging from 0.9 to 1.3%. The results additionally demonstrate that the sorption percentage of the PFAS examined onto the soil followed the order of (PFOS > PFOA > PFHxS > PFBS). The order of sorption percentage of the PFAS studied was consistent with the solubility and the octanol-water coefficient (log K_{ow}) of each compound (Table S3). Therefore, as PFOS is the most hydrophobic and least soluble in water, the percentage of sorption reached 56%. However, this percentage reduces by over four times for PFOA (13.8%) and PFHxS (12%) and by more than ten times for PFBS (3.3%). The significant sorption of PFOS compared to PFOA is due to the presence of additional carbon in the hydrophobic chain. Even though the PFHxS perfluorinated chain is shorter than PFOA, the log K_{ow} values are very comparable, (4.34 to 4.59) leading to a slight variation in sorption percentage. PFBS showed the lowest sorption percentage because of its shorter perfluorinated chain, which explains its lesser hydrophobic nature on the one hand and its greater water solubility on the other hand. Given the TOC content (1.14%), the main mechanism of PFAS sorption onto soil was the

interaction between the hydrophobic tail and the soil organic matter, as has been demonstrated in several studies [80,66,81,70,82]. In terms of head groups, sulfonates exhibited notably greater sorption affinity compared to their carboxylate analogs with equivalent -CF_2- chain length which is also consistent with previous studies [76,83].

Several other factors can influence the sorption of PFAS such as the pH, the clay mineral (kaolinite), and the ionic strengths of inorganic salts such as $CaCl_2$. The effect of cations will be discussed in detail in the following section. The measured pH of the soil was 6.5, indicating slightly acidic conditions. In this pH range, less negatively charged soil enhances the attraction between PFAS and soil particles leading to an increase in PFAS sorption [77,83]. As noted by Vierke et al. [84], the pKa values for the 4 PFAS tested in this study are relatively low (typically < 3.5), which indicates that these compounds predominantly existed in their deprotonated state [85]. According to Loganathan and Wilson [86], long-chain perfluoro sulfonic acids (PFSA) and perfluoro carboxylic acids (PFCA) have an affinity to be strongly sorbed on the hydroxylated kaolinite surface, as a result of the direct coordination occurring between the hydroxyl groups on the surface and the perfluoroalkyl acids (PFAA).

3.3. Effect of cations on PFAS sorption/desorption behavior

Given its complex chemical structure, PFAS may interact with soils through a variety of sorption mechanisms in the presence of cations such as Ca^{2+}. Electrostatic interactions with mineral and organic adsorbent surfaces, along with hydrophobic effects with organic carbon (OC) in soil are primarily responsible for these immobilization mechanisms [59,76]. Several mechanisms contribute to the enhancement of PFAS sorption on soil in the presence of $CaCl_2$ as presented by Cai et al. [85] such as (1) salting-out effect, (2) cation bridging, (3) reduction of repulsive forces among PFAS molecules as well as between PFAS and negatively charged surfaces and (4) enhancing the hydrophobic interaction of PFAS tail with organic matter [83].

The salting-out effect (SEO) [87] and the Ca-bridging effect [88] may contribute to both the reduction in PFAS desorption and the enhancement of PFAS sorption in the presence of $CaCl_2$ solution. Organic matter in the soil may become glassier due to the activity of Ca^{2+} ions in the solution, which may serve as cross-linking agents [89]. Thus, while concurrently decreasing the desorption of PFAS, this process increases irreversibility. Several studies demonstrated that the presence of cations such as Ca^{2+} raises the sorption rate of PFAS onto soil by the cation bridge mechanism [85,77,88,90]. The sorption behavior of different organic pollutants can be affected by the presence of salt in water due to the modification of the electrical state of the sorbent surface and the reduction of the activity of water [89]. Salt ions, on the other hand, may electrostatically interact with water molecules, leading to a decrease in the activity of water and consequently to lower solubility of organic pollutants via the SEO mechanism [91,92]. It has been reported that PFOS solubility decreases from 570 $mg.L^{-1}$ in pure water to 25 $mg.L^{-1}$ in filtered seawater [93] and to 307 $mg.L^{-1}$ in 0.005 $mol.L^{-1}$ $CaCl_2$ solution [88].

Electrostatic forces and hydrophobic interactions further influence PFAS behavior at the soil interface [94]. Even in the absence of polyvalent cations, hydrophobic forces significantly contribute to PFAS sorption, particularly for longer-chain PFAS and in soils richer in OC [95]. However, the presence of cations like Ca^{2+} enhances sorption by reducing electrostatic repulsion among PFAS molecules and between PFAS and soil surfaces, allowing for better orientation and packing of PFAS molecules [59,96]. This effect is particularly pronounced for long-chain PFAS, which exhibit stronger hydrophobic interactions and greater sorption in the presence of Ca^{2+}. In contrast, short-chain PFAS experience a smaller increase in sorption with rising ionic strength because the suppression of repulsive forces by Ca^{2+} is insufficient to significantly enhance their hydrophobicity and, therefore, their sorption. For instance, Cai et al. [85] found that short-chain PFSA and PFCA exhibited very low sorption percentages even in the presence of high ionic strength. Furthermore, Chen et al. [66] reported that the addition of 10 mM $CaCl_2$ to a PFAS solution reduces the negative charge of the soil, thereby enhancing the sorption of PFOS and PFOA.

3.4. Desorption batch experiments

To examine the effectiveness of various recovery solutions, a batch-scale experiment was conducted using water with and without $CaCl_2$, and ethanol (50% v/v) with and without XG solutions at varying concentrations. Fig. 4 depicts the recovery percentage of PFOA, PFOS, PFHxS, and PFBS at different time intervals. For each recovery solution, the desorption kinetics are fast during the first 30 min, then remain very slow until equilibrium after 24 h of agitation. PFAS desorption from soil was a result of a competition between the anionic head and the hydrophobic tail. The presence of organic matter has a major influence on the mobility of PFAS from soil to the aqueous phase and subsequently decreases PFAS desorption [97]. Following a 24-hour of agitation in water, the percentage of PFAS desorbed was 44.5 ± 2%, 79 ± 6%, 82 ± 7%, and 100 ± 11% for PFOS, PFOA, PFHxS and PFBS, respectively. Both PFOA and PFOS have 8 carbons, but the eighth carbon in PFOA's functional group shortens the chain, making it less hydrophobic and more mobile. These features result in higher PFOA mobilization than PFOS. Although PFOA is two times more soluble than PFHxS, their similar log K_{ow} and K_d values as discussed in previous sections, lead to comparable desorption percentages. The lowest sorption of PFBS and its highest solubility explained the desorption percentage obtained.

As illustrated in Fig. 4, mixing water with ethanol at the same ratio (1:1) led to a major enhancement in PFAS recovery especially for PFOS, as its desorption percentage increased two times to reach 95.5 ± 2.5%. The effect of ethanol in enhancing other PFAS desorption was minor, as PFOA and PFHxS removals increased by 15% to reach 97.5 ± 4.5%, and 97.9 ± 1.5%. This shows that the solubility of PFAS in ethanol (50% v/v) is higher than that of pure water. These results were comparable to the literature. Deng et al. [43], used ethanol (50% v/v) for the regeneration of activated carbon contaminated by PFOS and discovered that after 24 h, ethanol was capable of removing over 98% of PFOS. Similar results were also reported by Wang et al. [98], as (50% v/v) ethanol was able to regenerate over 85% of PFOS from GAC and anion-exchange resins.

Adding three different concentrations of xanthan gum into (50% v/v) ethanol resulted in an additional 3% increase in recovery, achieving 99 ± 2% efficiency for PFOS, PFOA, and PFHxS. The slight decrease in the recovery percentage of PFBS 4 to 8% is attributed to minimal sorption on the soil. These findings suggest that the concentration of xanthan gum has negligible impact on the effectiveness of 50% ethanol in PFAS desorption, as the recovery percentage remains consistent across all samples.

In addition, we tested the effect of $CaCl_2$ on the recovery of PFAS and found that increasing the ionic strength of the aqueous solution significantly affects the desorption of the shortest PFAS in this study (C4). This resulted in a reduction in PFBS recovery of 35%, 15% for PFOA and PFHxS, and 4% for PFOS. The observed reduction in PFAS desorption percentages with changes in ionic strength can be attributed to the distinct mechanisms influencing PFAS sorption, as discussed in Section 3.3. The pH of the soil remained relatively unchanged after the injection of various flushing solutions, suggesting that the observed results were not influenced by fluctuations in pH.

The mixture investigated for PFAS desorption in the 1D column experiment is the mixture of xanthan and ethanol (XE), where, xanthan (XG) is presented at its lowest concentration of 0.05% w/w. This choice was based on previous evidence indicating that ethanol did not affect the shear thinning behavior of the xanthan gum solution. Additionally, it has been found that the addition of different concentrations of XG to ethanol solutions enhanced the recovery percentage of the PFAS.

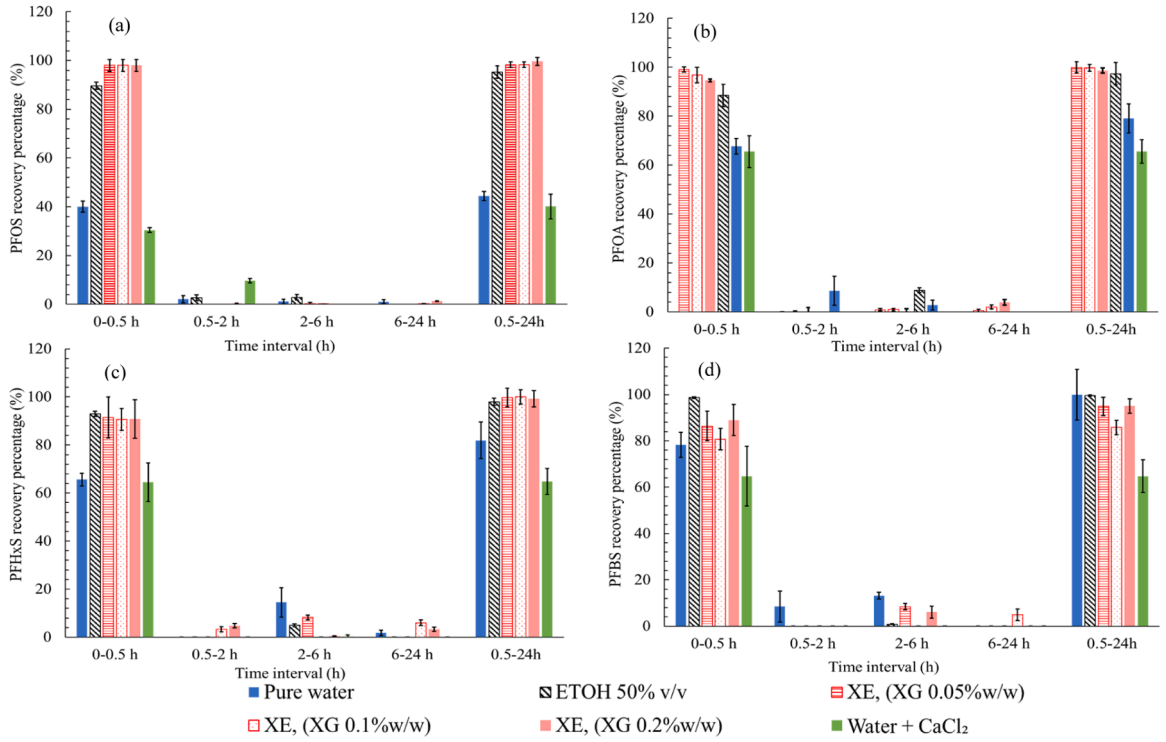

Fig. 4. Recovery percentage of (a) PFOS, (b) PFOA, (c) PFHxS, and (d) PFBS at different time intervals and recovery solutions. Notes: ETOH = Ethanol; XG = Xanthan Gum; XE = xanthan-ethanol mixture. Each data point and error bars are means and standard deviations of triplicates, respectively.

3.5. 1D column sorption and desorption experiments

3.5.1. Sorption experiments

The sorption and desorption experiments of the mixture of PFAS at a concentration of 5 mg.L^{-1} were conducted at a 1D decimetric scale. To highlight the effect of adding ethanol (50% v/v) to water and subsequently the polymer on the PFAS recovery, each single PFAS breakthrough curve (BTC) is presented in Fig. 5 alone as a function of pore volume injected (PV). The transition from PFAS injection to PFAS-free solution flushing is represented by the black dotted line for the four graphs. The tails of the BTCs for individual PFAS overlapped well for every column, which demonstrated the accurate repeatability of the experiments (standard deviation lower than 4%). The percentage of PFAS sorption is presented in Fig. S1 in supplementary materials. Following the experimental outcomes, PFBS was the most rapidly eluted compound at 0.6 PV. Its fast breakthrough confirmed that this compound was the last sorbed. PFHxS and PFOA had a simultaneous breakthrough at 0.75 PV. The retardation to achieve the complete breakthrough at 3.3 PV for PFOA compared to 2.8 PV for PFHxS indicates higher sorption in the porous media. PFOS was the most sorbed compound, in terms of BTC tail, time, and stabilization as its elution was at 2.5 PV, and showed no complete breakthrough after 5.2 PV of injection ($C/C_0 = 0.4$). These findings correlated with the physio-chemical properties of each PFAS and were consistent with batch sorption tests. PFBS's high water solubility and low hydrophobicity explained its lower sorption in soil (26 ± 3%). The simultaneous breakthrough of PFOA and PFHxS was due to the higher water solubility of PFOA, which facilitated its mobilization. Although it remains more hydrophobic than PFHxS (C8 to C6), their sorption percentages were comparable at equilibrium (40 ± 2% to 36 ± 4%) as demonstrated in batch sorption (Section 3.2). PFOS's long carbon chain and lower water solubility enable it to be strongly retained by the porous medium, resulting in a slower breakthrough and a strong sorption percentage (89 ± 3%). The high sorption is attributed to the variation in PFAS chain lengths, which results in differing levels of hydrophobicity [83]. Other factors that may influence the sorption behavior of each PFAS include the functional group of the head, with the sulfonate head group leading to stronger sorption compared to the carboxylic group [99], and the presence of Ca^{2+} in the solution, as previously discussed. The breakthrough curve indicates how PFBS behaves in environmental matrices, as its shorter chain length (C4) gives it a percolating capacity that makes it more mobile in groundwater compared to longer-chain PFAS.

3.5.2. Desorption experiments

Various flushing solutions, comprising ethanol with and without xanthan gum, pure water, and water with $CaCl_2$, underwent examination to assess their effectiveness in removing PFAS after sorption experiments. As shown in Fig. 5, PFAS delayed for approximately 1PV has a response for the desorption solutions used. A similar trend of breakthrough behavior for PFAS was noticed for all solutions except salty water.

The rate of decrease in PFAS concentration during the injection of water with $CaCl_2$ was influenced by the hydrophobicity of each compound. For instance, PFBS exhibited a more rapid decrease in concentrations. The relative concentration of PFOS required the entire injection period to decline to 20% of its initial sorption level. The time required for PFOA to reach C/C_0 nearly zero was higher than PFHxS for more than 1PV. Zhang et al. [100] demonstrated that the presence of divalent cations such as Ca^{2+} significantly enhances the sorption and retardation of PFOA in soil compared to monovalent cations like Na^{+}. This suggests that the presence of $CaCl_2$ in water reduces the solubility of PFAS molecules through the salting-out effect, thereby enhancing their sorption onto soil particles due to the cation bridging effect and reduction in repulsive forces. As discussed in Section 3.3, this process influences the transport of PFAS molecules in the porous medium leading to more effective retention and reduced mobility.

However, an increase in concentrations (peak) for long-chain PFAS after their breakthrough was noticed in water and ethanol with and without XG. The intensity and the area of the peak obtained after flushing with water became lower and tighter while the carbon chain

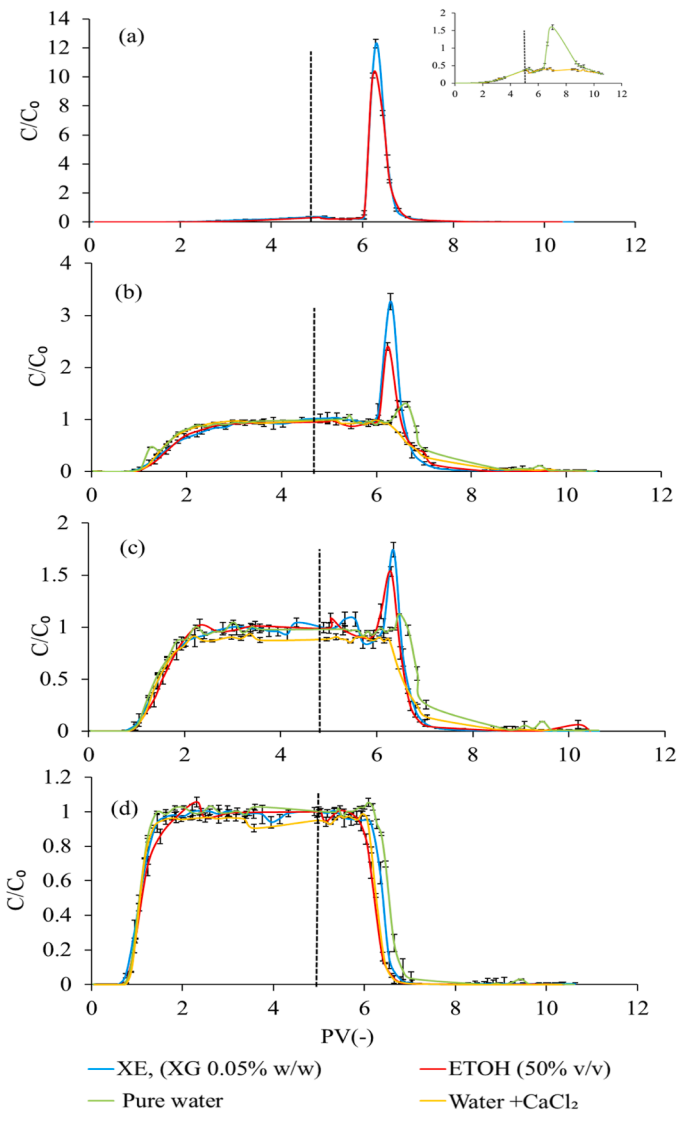

Fig. 5. Column breakthrough curves for (a) PFOS, (b) PFOA, (c) PFHxS, and (d) PFBS in soil. The transition from PFAS injection to PFAS-free solution flushing is represented by the vertical black dotted line. Each data point and error bars are means and standard deviations of triplicates, respectively.

and hydrophobicity of PFAS decreased (Table S4 in Supplementary materials). This issue is addressed in section 3.5.3. Furthermore, the effluent concentration of PFOS did not reach zero after complete water injection, which was not the case for other PFAS even if some of them delayed more than others to reach this value. The elution time of PFAS was faster in ethanol (50% v/v) with and without XG than in water. The effect of time elution was more noticeable for longer-chain PFAS (C ≥ 6). PFOS (C = 8) eluted for 0.3PV faster in ethanol solutions than in water. PFOA (C=8) and PFHxS (C=6) showed a synchronous breakthrough in ethanol solutions which was faster than in water for 0.2PV and 0.25 PV. This faster breakthrough suggested that adding ethanol (50% v/v) to water increases the solubility of PFAS, and enhances solubility forces versus hydrophobic forces. Lauwers et al. [101] showed that PFAS's hydrophobic tail can be solvated by organic solvents such as ethanol, making the hydrophobic interaction weaker. When comparing the peaks of long-chain compounds obtained after flushing with ethanol (red color) and ethanol-polymer mixture (blue color), the concentrations of PFOS and PFHxS in ethanol–polymer eluent were 20% to those in ethanol. In the case of PFOA, the ratio was almost 40%. These results indicate that transport of the carboxylic functional group was twice more enhanced than sulfonate groups. This difference is due to the weaker electrostatic interaction between carboxylate PFAS and the sorbent, leading to a lower sorption affinity for PFCA compared to PFSA [102].

One of the main issues in groundwater remediation is density-driven flow. Overridden flow occurs when a less dense fluid displaces a denser fluid, while under ridden flow happens when a denser fluid displaces a less dense fluid. Taylor et al. [103] in a series of two-dimensional experiments, observed that even a minor density difference (0.008 g/mL) between an injecting ethanol-surfactant mixture and water near a perchloroethylene (PCE)-contaminated zone can result in density-overridden flow. Grubb and Sitar, [104], during ethanol injection in two-dimensional uniform sand packs, observed ethanol gravity override with an increasing inclination angle of the ethanol front as invasion progressed. Alamooti et al. [105] demonstrated that to avoid density-driven issues during the displacement of dense non-aqueous phase liquid (DNAPL) in an unconfined aquifer, it is necessary to nullify gravity forces by balancing the density of the polymer and DNAPL. Although densifying the ethanol-water solution to match the water density could cancel out gravity forces, the addition of xanthan can increase viscous forces, thereby overcoming gravity-overridden flow [105] To avoid density-overridden flow during the remediation of PFAS-saturated soil, xanthan was added to an ethanol-water mixture.

To understand the density-driven flow, gravity number analysis can be used [105]. The gravity number is defined as the ratio of buoyancy forces to viscous forces, indicating the balance between them and determining the flow direction. It can be expressed as [106].

$$N_G = \frac{\Delta\rho g k}{v\mu} \tag{15}$$

where $\Delta\rho$ is the density difference (kg.m^{-3}), g is the gravitational acceleration (m.s^{-2}), k is the intrinsic permeability (m^2), v is the velocity magnitude of the invading phase (m.s^{-1}), μ is the viscosity of the invading phase (Pa.s). Alamooti et al. [105] demonstrated that to counteract gravity forces during the remediation of saturated soil, it is necessary to maintain the gravity number close to zero. In the context of ethanol mixture injection for PFAS mobilization, gravity number analysis shows that without polymer, the gravity number is approximately −3.62, indicating an overriding flow. However, when xanthan is added to the mixture, this value increases to around −0.009, which is near zero, representing an ideal condition for avoiding density-driven flow.

The PFAS recovery percentages were calculated according to Eq. 13. As depicted in Fig. 6, the recovery of PFAS increased proportionally with the addition of ethanol and polymer to a pure water solution. The presence of 50% v/v ethanol in water solution increased the recovery percentage by almost 20% to reach 94% for PFOA, 85% for PFHxS, and 84% for PFOS except for PFBS, as discussed earlier regarding its increased solubility. These results confirm the reported high recovery of PFOS and PFOA using ethanol to regenerate activated carbon [43,46]. The presence of xanthan gum in ethanol (50% v/v) enhanced the

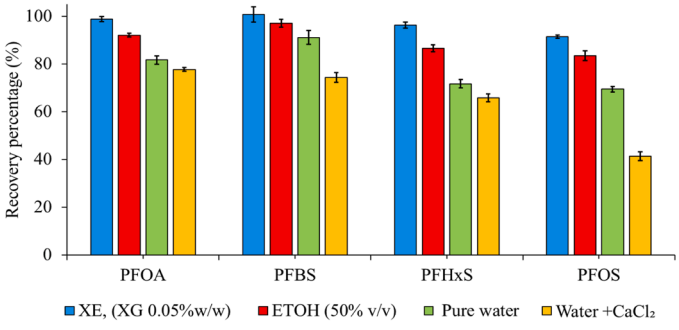

Fig. 6. Total PFAS recovery percentages after using different solutions in the 1D column.

recovery percentage to reach more than 92% for all PFAS, and this mixture represented a promising solution for in situ PFAS flushing. In addition, the presence of $CaCl_2$ in aqueous solution significantly reduces the desorption of PFSA compounds more compared to PFCA ones with PFOS showing a 28% reduction in recovery versus 4% for PFOA. This difference is attributed to the stronger Ca-bridging interactions between sulfonate groups and soil particles, as sulfonate possesses a higher negative charge density than carboxylate groups [107]. Similarly, Zhao et al. [108], reported that PFOA exhibited much lower sorption than PFOS due to the weaker Ca-bridging of PFCA with soil than PFSA.

3.6. 1D column modeling

The experimental and modeled (optimized) breakthrough curves (BTCs) of non-reactive tracer KBr are shown in the supplementary materials Fig. S2. The longitudinal dispersion coefficient is obtained by fitting the 1D convection-dispersion equation to the experimental result. The optimization problem and the convection-dispersion equation were solved using COMSOL Multiphysics. The optimized longitudinal dispersivity is $\alpha_L = 6.89 \times 10^{-3}$ m. As seen, the measured breakthrough curve shows a non-negligible long-time tail, which is often due to the presence of a low-velocity zone created during the packing.

We first examine the modeling of sorption tests. Then, desorption tests using water with $CaCl_2$ and XE mixture are simulated. This modeling work aims to (i) validate the use of the traditional convection-dispersion equation supplemented by a common sorption isotherm relation to reproduce the sorption tests, (ii) propose and validate a model to reproduce the desorption of PFAS using various fluids, including the ethanol/xanthan mixture.

3.6.1. Sorption in 1D column

Fig. 7 shows the measured and modeled breakthrough curves during the sorption steps for the four PFAS. The modeled curves are given either assuming no sorption or assuming sorption using the well-known Langmuir sorption isotherm model. In the case of sorption, the parameters required for the Langmuir sorption isotherm model are found by solving an optimization problem, taking into account the experimental data as the objective function, and the output of the convection-dispersion-adsorption model as the variable to be optimized.

Among the four studied PFAS, the PFBS is the only one for which the measured elution curve can be accurately reproduced by neglecting the sorption to the solid particles. This is consistent with the batch results, as well as with the previous discussion of the 1D column experiments. The Langmuir sorption isotherm model allows an acceptable reproduction of three of the four experimentally obtained breakthrough curves, using the parameter values summarized in Table S5 in supplementary materials. Indeed, the PFOS breakthrough curve could not be reproduced, at least using a set of parameter values in line with the work of [109]. This finding indicates that the hypothesis of instantaneous partitioning of the solute between aqueous and solid phases might not be appropriate (i.e., non-equilibrium sorption should be favored), regarding PFOS transport in our system, which is also in line with observation from the literature [60]. PFOS is known to exhibit nonlinear, rate-limited, and extended long-tail breakthrough curves [62]. Consequently, modeling approaches such as the two-domain or the continuous distribution of sorption domains are more appropriate, as demonstrated by the authors of the above reference.

Significantly, the fact that no competition was observed between the PFAS on the sorption sites meant that the breakthrough curves obtained by the model were able to reproduce the observations well, even though the model was run for each individual PFAS, unlike the experiments, which were carried out by injecting the 4 PFAS together. In summary, breakthrough curves obtained during the experiments can be numerically reproduced using the convection-dispersion-sorption equation, using the Langmuir sorption isotherm, except for PFOS. The parameter values for the Langmuir isotherm, obtained by optimization, are in line with values in the literature [109].

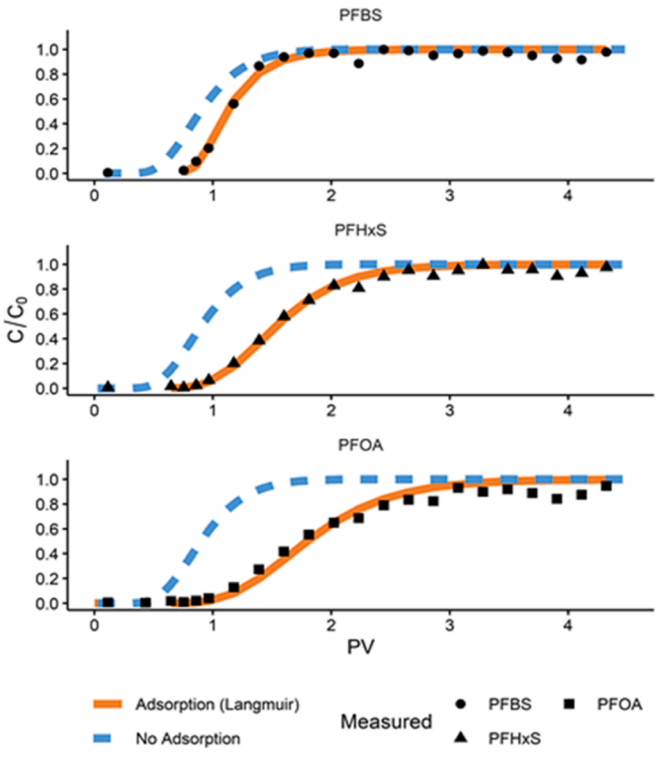

Fig. 7. Measured and modeled breakthrough curves during 1D column sorption tests. Modeled breakthrough curves are presented with and without taking into account sorption. When sorption is considered, the Langmuir sorption isotherm model is used. The two parameters from the Langmuir isotherm are obtained by solving the optimization problem based on the experimental data. The accuracy of fitting (residual standard error RSE) is presented in Fig. S3 (Supplementary materials) for optimized runs.

3.6.2. Desorption in 1D column using water with $CaCl_2$

We first model the desorption tests using the same background solution as for the sorption tests, i.e., ultrapure water with $CaCl_2$. The same model is applied (convection-dispersion-sorption equation), again using the Langmuir sorption isotherm. Doing so, two options are possible, i.e., assuming no sorption hysteresis and using the same parameters as in Table S4, or solving again the optimization problem to find the best set of parameter values. Both solutions have been applied, as shown in Fig. 8, which shows measured and modeled (either with the same parameter values or with optimized ones) desorption curves for all three PFAS (PFOA, PFHxS, and PFBS). As for the sorption models, the PFOS breakthrough curves cannot be reproduced using physically meaningful parameter values.

As shown, little sorption hysteresis is observed as the optimized and non-optimized breakthrough curves are similar. As with the modeling of the sorption tests, the convection-dispersion-sorption equation, using Langmuir sorption isotherm, can reproduce the data satisfactorily.

water + $CaCl_2$ (same fluid used as background fluid for the sorption tests). Modeled elution curves are presented with and without optimization, i.e., using the same parameter values as with the sorption tests (no optimization), or by solving again the optimization problem. The Langmuir sorption isotherm model is used. The accuracy of fitting (residual standard error RSE) is presented in Fig. S3 (Supplementary materials) for optimized runs.

3.6.3. Desorption in 1D column using ETOH (50% v/v) and XE mixture

As previously discussed, the experimental desorption breakthrough

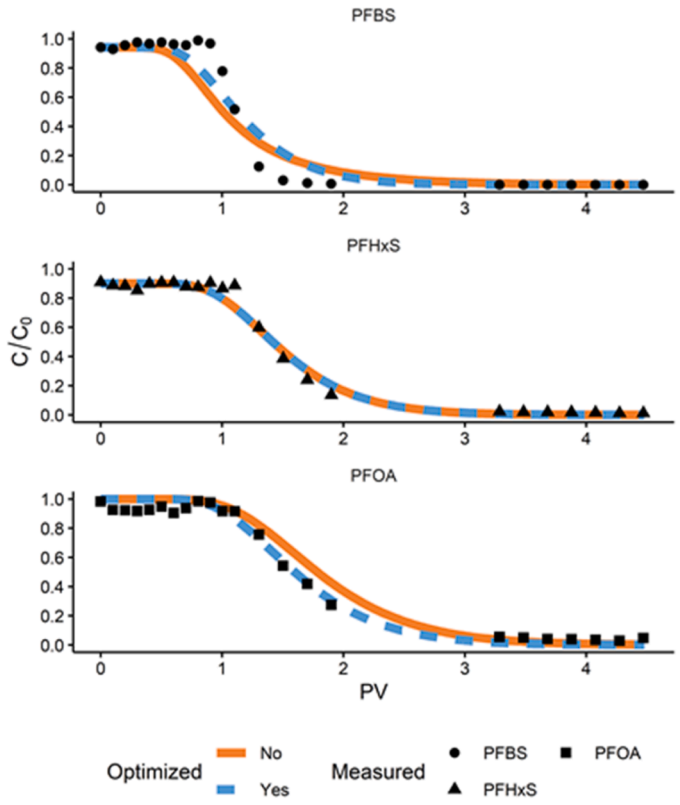

Fig. 8. Measured and modeled elution curves during 1D column desorption tests using ultrapure.

curves show a concentration overshoot ($C/C_0 > 1$), except for the PFBS, during desorption using ETOH (50% v/v) and XE mixture. A concentration overshoot is sometimes observed during the sorption stage, due to competitive behavior in multicomponent solute transport. However, the observed overshoot is not suitable for modeling using a competitive sorption model because the excess mass of solute comes from PFAS solubility contrast between different fluid phases, namely the background sorption solution (water with $CaCl_2$) that is still present as sorbed water and is loaded with PFAS, and the PFAS solubility in the desorption solutions especially those involving ethanol. It is thus not related to competition for sorption sites between PFAS themselves or between PFAS and ethanol.

Given this and the lack of knowledge of the mass of adsorbed water and its spatial distribution, the proposed ad-hoc model is both phenomenological and empirical. Specifically, we acknowledge that the presence of ethanol is the main driver of enhanced solubilization by introducing the ethanol concentration as a primary variable to be solved. The transport of ethanol obeys the convection-dispersion equation, and sorption phenomena are neglected. A source term proportional to the gradient of the ethanol concentration is then added to the PFAS transport equation. The rationale for this is that the breakthrough curves with overshoot show that the excess mass of PFAS is concentrated around the front of the injected/displaced fluid (the overshoot occurred during 0.5 PV or less).

Fig. 9a shows the elution curves (modeled and measured) which exhibit a concentration overshoot during desorption by ethanol (50% v/v). These are PFHxS (left panel), and PFOA (right panel). PFBS showed no concentration overshoot and can therefore be modeled with the same approach used for water with $CaCl_2$ desorption, but the Langmuir parameters are different. As for the sorption tests, PFOS cannot be modeled, at least with parameter values in the range found in the literature. As shown, it is possible to satisfactorily reproduce the measured data, including the overshoot part, with the proposed ad hoc model. To do so, the magnitude of the factor in the mass source term should be adjusted (optimized), and its value directly controls the magnitude of the overshoot peak. Langmuir parameters are also control variables for the optimization problem, as for previous cases. One can observe a delay in the arrival of the peak compared with the measurements, which may be explained by the fact that only the convective displacement of the ethanol is taken into account (no delay and insignificant dispersion), in order to reproduce the piston-like displacement.

Finally, Fig. 9b shows the measured and modeled elution curves for the PFAS during desorption by XE mixture. Compared to the previous case (ETOH desorption), we also plot the modeled elution curves obtained using the Langmuir sorption isotherm only (with optimization of the parameter values – dashed lines); i.e., without mass source term in the PFAS transport equation. The proposed ad-hoc model successfully captured the overshoot, unlike the basic model. Again, the delay in peak arrival between modeled and measured data can be observed. However, unlike the previous case with ETOH, the model cannot reproduce a sharp decrease in the normalized concentration after the peak is reached. It means that the mixing zone when the excess mass of PFAS is located is even thinner than during the ETOH desorption. However, as dispersivity is already insignificant for this latter, it is not possible here to reproduce an even thinner front.

4. Considerations for a real-world application of PFAS soil flushing technique

The remediation efficacy of PFAS-contaminated soils is affected by several influencing factors including contamination aging effect and soil composition. PFAS contamination aging can reduce the removal efficiency by flushing solutions due to reduced accessibility to the pollutants [110]. Soil composition is also concerned, as the higher the organic matter content the smother the beneficial efficacity of the flushing solutions. The introduction of ethanol as a flushing solution, to the soil ecosystems can modify microbial communities and soil properties. At moderate concentrations, ethanol enhances the biodegradation of other organic compounds, while serving as a carbon source, and promotes rapid activation of microbial respiration [111,112]. Furthermore, ethanol offers good remediation yields, but its injection as an aqueous solution can be inconsistent in heterogeneous field environments. Xanthan gum solution as a shear-thinning fluid ensures uniform ethanol distribution in varied soil conditions, thereby maintaining high remediation yields [113]. This biodegradable polymer can be effectively broken down in aerobic conditions by soil bacteria and fungi [114].

Although no large-scale application of polymer/ethanol injection for PFAS-contaminated soils has been reported, surfactant and solvent injections have been implemented for organic compound remediation [115]. Full-scale implementation would follow conventional flushing procedures, with injection and recovery wells handling viscous solutions. Effluents could be treated via distillation [116], membranes [117], or biological treatments [118]. PFAS in the effluent should be concentrated using membrane processes or activated carbon before destruction by incineration or advanced chemical treatments [119].

In this study, we evaluated the effectiveness of a mixture of ethanol and 0.5 g/L of xanthan gum solution, in desorbing and solubilizing a PFAS mixture from sandy soil, representative of alluvial French soil. The concentration of xanthan gum employed is lower than the typical range of 1–1.5% for soil treatment [120,121] further underscoring its cost efficiency. This soil type, with high permeability and porosity, allowed for effective simulation of the in-situ flushing method. Batch experiments showed rapid PFAS removal within the first 30 min. A flow rate of 2 mL/min (equivalent to 2.3 m/day) efficiently desorbed and removed PFAS within less than two pore volumes of injection time, approximately five hours. Injection rates would need adjustment for soils with different compositions or lower permeability. The shear-thinning behavior of the non-Newtonian fluid in the flushing solution enhances flow, as shown in previous studies on organic contaminants [105]. Specialized pumps

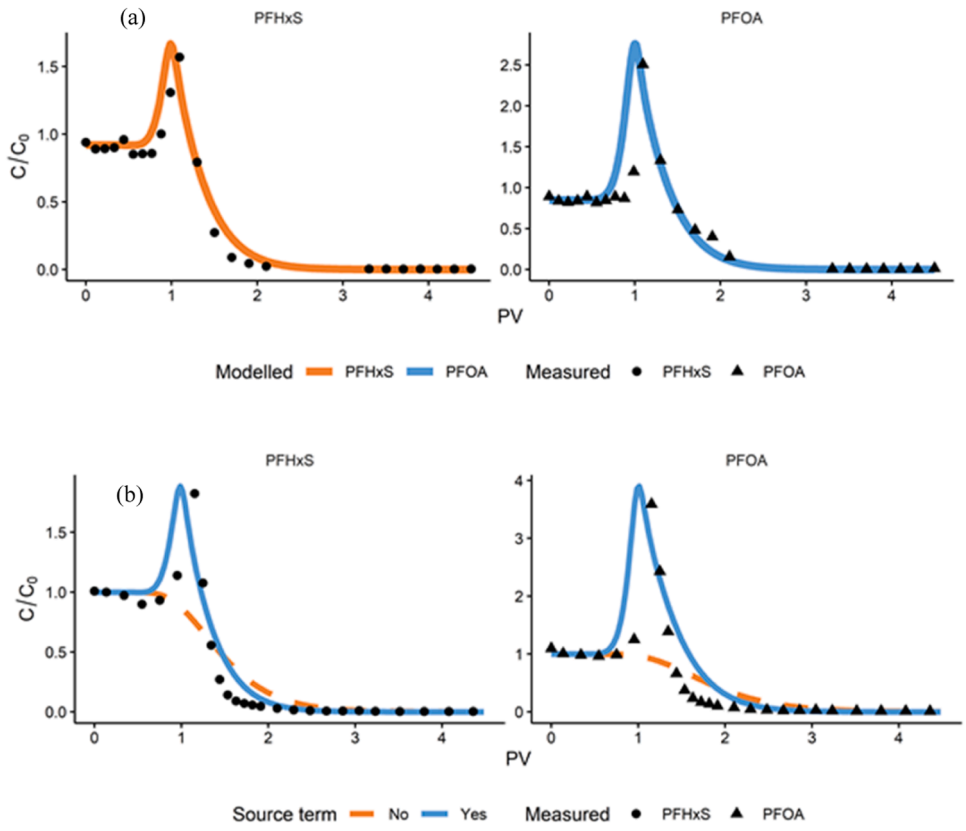

Fig. 9. Measured and modeled elution curves showing a concentration overshoot during 1D column desorption tests using ETOH (50% v/v). Modeled elution curves are obtained by adding a source term that depends on the ethanol concentration gradient (a). Measured and modeled elution curves showing concentration overshoot during 1D column desorption tests using XE. Modeled elution curvesare presented with and without a source term, i.e., using Langmuir sorption isotherm only (no source term), or by adding a source term that depends on the ethanol concentration gradient (b).The accuracy of fitting (RSE) is presented in Figure S3 (supplementary materials).

would be necessary to handle the injection of the viscous solution in real-site applications. The injection and recovery of the solution can be performed using an in situ rinsing method, as described in the study by Maire et al. [122], similar to classical flushing on a real field scale.

5. Conclusion

This study aimed to assess the effectiveness of mixing xanthan gum, a bio-polymer with ethanol (50% v/v) to enhance the recovery of various PFAS carbon-chain compounds from soil. For this purpose, rheological experiments confirmed that ethanol did not affect the shear-thinning behavior of the polymer across different xanthan gum concentrations. Batch-scale experiments of PFAS sorption indicated a positive correlation between solubility and hydrophobicity properties and the achieved sorption percentages. Desorption batch experiments using ethanol (50% v/v) resulted in over 95% recovery of all four PFAS compounds, with a 3% increase in desorption yield observed after incorporating the polymer, regardless of its concentration. Additionally, increasing the ionic strength (10 mM of $CaCl_2$) of water decreased PFAS solubility and, consequently, removal percentages. The results facilitated the selection of the polymer concentration in the ethanol-xanthan gum mixture. The chosen mixture was tested in 1D column experiments, and its efficiency was compared to that of ethanol and water. Notably, the sorption magnitudes measured in the column experiments closely matched those obtained in the batch experiments. The breakthrough of long-chain PFAS occurred more rapidly in ethanol with and without XG compared to water, owing to the increased solubility of PFAS. The overshoot in PFAS concentrations (peak) observed after flushing with water was influenced by the hydrophobicity of each compound, whereas in the xanthan gum–ethanol mixture, long-chain PFAS peaks were higher than in ethanol alone, indicating stable displacement and uniform ethanol transport in the soil. The addition of ethanol to water had a significant effect on the percentage of PFAS recovery as it reached 85% for PFOS and PFHxS, 94% for PFOA, and 96% for PFBS. The mixture of ethanol (50% v/v) with xanthan gum enhanced the recovery percentage to reach more than 97% for PFOA, PFBS, PFHxS, and 92% for PFOS.

Furthermore, numerical modeling shows that the convection-dispersion-sorption equation using the Langmuir sorption isotherm allows to reproduce the breakthrough curves of PFOA, PFHxS, and PFBS (the model is also satisfactory by neglecting sorption in this case), but not of PFOS. Although the experiments were performed with a mixture of all PFAS, the lack of competition for sorption sites allows the data to be reproduced by simulating the PFAS transport separately for each compound. We also proposed an ad-hoc model to reproduce the concentration overshoot during the xanthan with ethanol desorption tests. The model is based on an additional transport equation for the ethanol concentration, and a source term proportional to the ethanol concentration gradient is added to the PFAS transport equation. Although the model is ad-hoc, it satisfactorily captures the concentration overshoot, as it is based on a hypothesis of the underlying physicochemical mechanism that causes the overshoot, i.e., the contrast in PFAS solubility between the background solutions used for sorption tests, and the solution used for desorption with 50% ethanol.

Based on these findings, the in-situ flushing with the polymer-ethanol mixture presents a promising approach for efficient PFAS recovery from soil, offering ease of application through subsurface injection. Future research should explore the application of this mixture in multi-layer systems to better understand the impact of non-Newtonian properties on ethanol transport and, consequently, PFAS recovery efficiency.

Environmental implication

The growing environmental concern regarding the contamination by per- and polyfluoroalkyl substances (PFAS), persistent synthetic chemicals that can infiltrate soil and groundwater, is posing threats to ecosystems and human health. To address this concern, an in-situ remediation method was explored. Soil flushing is a remediation technique designed to remove contaminants from soil by injecting a blend comprising biodegradable xanthan gum and ethanol to recover PFAS from polluted soils. Controlled column experiments were conducted, revealing improved PFAS desorption due to the homogeneous mobilization induced by the polymer in the ethanol solution. Therefore, soil flushing may significantly contribute to mitigating environmental risks.

CRediT authorship contribution statement

Ali Batikh: Conceptualization, Methodology, Investigation, Validation, Formal analysis, Writing – original draft, Data Curation, Visualization. **Stéfan Colombano**: Conceptualization, Methodology, Validation, Writing - Review & Editing, Supervision, Project administration, Funding acquisition. **Maxime Cochennec**: Methodology, Data curation, Writing - Review & Editing. **Dorian Davarzani**: Writing - Review & Editing, Supervision. **Arnault Perrault**: Project administration, Funding acquisition. **Julie Lions**: Project administration, Funding acquisition. **Julien Grandclément**: Project administration, Supervision, Writing - Review & Editing. **Dominique Guyonnet**: Writing - Review & Editing, Funding acquisition. **Anne Togola**: Writing - Review & Editing, Funding acquisition. **Clément Zornig**: Ressources. **Nicolas Devau**: Formal analysis, Funding acquisition. **Fabien Lion**: Ressources. **Amir Alamooti**: Writing - Review & Editing. **Sébastien Bristeau**: Formal Analysis. **Mohamed Djemil**: Formal Analysis. **Eric D. van Hullebusch**: Conceptualization, Methodology, Validation, Writing - Review & Editing, Supervision, Project administration, Funding acquisition.

Declaration of Competing Interest

The authors declare that they have no known competing financial interests or personal relationships that could have appeared to influence the work reported in this paper.

Acknowledgments

The research leading to these results has received funding from the European Union H2020 Programme (H2020/2014–2020) under grant agreement n° 101036449. This work was carried out within the framework of the PROMISCES project. The authors would like to thank BRGM (French Geological Survey), COLAS ENVIRONNEMENT, and ANRT (Association Nationale de la Recherche et de la Technologie) for co-funding the project. The authors also acknowledge the financial support provided to the PIVOTS project by the “Region Centre-Val de Loire” and the European Regional Development Fund.

Appendix A. Supporting information

Supplementary data associated with this article can be found in the online version at doi:10.1016/j.jhazmat.2024.136496.

Data availability

Data will be made available on request.

References

[1] Gagliano, E., Sgroi, M., Falciglia, P.P., Vagliasindi, F.G.A., Roccaro, P., 2019. Removal of poly- and perfluoroalkyl substances (PFAS) from water by adsorption: Role of PFAS chain length, effect of organic matter and challenges in adsorbent regeneration. Water Res 171, 115381.

[2] Taniyasu, S., Kannan, K., So, M.K., Gulkowska, A., Sinclair, E., Okazawa, T., Yamashita, N., 2005. Analysis of fluorotelomer alcohols, fluorotelomer acids, and short- and long-chain perfluorinated acids in water and biota. J Chromatogr A 1093 (1-2), 89–97.

[3] Houde, M., De Silva, A.O., Muir, D.C.G., Letcher, R.J., 2011. Monitoring of Perfluorinated Compounds in Aquatic Biota: An Updated Review. Environ Sci Technol 45 (19), 7962–7973. https://doi.org/10.1021/es104326w.

[4] Mazumder, N.-U.-S., Hossain, M.T., Jahura, F.T., Girase, A., Hall, A.S., Lu, J., Ormond, R.B., 2023. Firefighters’ exposure to per-and polyfluoroalkyl substances (PFAS) as an occupational hazard: A review. Front Mater 10. https://doi.org/10.3389/fmats.2023.1143411.

[5] Sun, R., Babalol, S., Ni, R., Dolatabad, A.A., Cao, J., Xiao, F., 2024. Efficient and fast remediation of soil contaminated by per- and polyfluoroalkyl substances (PFAS) by high-frequency heating. J Hazard Mater 463, 132660. https://doi.org/10.1016/j.jhazmat.2023.132660.

[6] Brunn, H., Arnold, G., Körner, W., Rippen, G., Steinhäuser, K.G., Valentin, I., 2023. PFAS: forever chemicals—Persistent, bioaccumulative and mobile. Reviewing the status and the need for their phase out and remediation of contaminated sites. Environ Sci Eur 35 (1), 20. https://doi.org/10.1186/s12302-023-00721-8.

[7] Cousins, I.T., DeWitt, J.C., Glüge, J., Goldenman, G., Herzke, D., Lohmann, R., Ng, C.A., Scheringer, M., Wang, Z., 2020. The high persistence of PFAS is sufficient for their management as a chemical class. Environ Sci: Process Impacts 22 (12), 2307–2312. https://doi.org/10.1039/D0EM00355G.

[8] Johnson, G.R., Brusseau, M.L., Carroll, K.C., Tick, G.R., Duncan, C.M., 2022. Global distributions, source-type dependencies, and concentration ranges of per- and polyfluoroalkyl substances in groundwater. Sci Total Environ 841, 156602. https://doi.org/10.1016/j.scitotenv.2022.156602.

[9] Podder, A., Sadmani, A.H.M.A., Reinhart, D., Chang, N.-B., Goel, R., 2021. Per and poly-fluoroalkyl substances (PFAS) as a contaminant of emerging concern in surface water: A transboundary review of their occurrences and toxicity effects. J Hazard Mater 419, 126361. https://doi.org/10.1016/j.jhazmat.2021.126361.

[10] USEPA. (2024). Drinking Water Treatability Database.

[11] European Commission. (2018). Proposal for a Directive of the European Parliament and of the Council on the Quality of Water Intended for Human Consumption (Recast).

[12] Qian, J., Shen, M., Wang, P., Wang, C., Hu, J., Hou, J., Ao, Y., Zheng, H., Li, K., Liu, J., 2017. Co-adsorption of perfluorooctane sulfonate and phosphate on boehmite: Influence of temperature, phosphate initial concentration and pH. Ecotoxicol Environ Saf 137, 71–77. https://doi.org/10.1016/j.ecoenv.2016.11.026.

[13] Zhou, Y., Hu, L.-W., Qian, Z. (Min), Chang, J.-J., King, C., Paul, G., Lin, S., Chen, P.-C., Lee, Y.L., Dong, G.-H., 2016. Association of perfluoroalkyl substances exposure with reproductive hormone levels in adolescents: By sex status. Environ Int 94, 189–195. https://doi.org/10.1016/j.envint.2016.05.018.

[14] Niarchos, G., Ahrens, L., Kleja, D.B., Fagerlund, F., 2022. Per- and polyfluoroalkyl substance (PFAS) retention by colloidal activated carbon (CAC) using dynamic column experiments. Environ Pollut 308, 119667. https://doi.org/10.1016/j.envpol.2022.119667.

[15] Pepper, I.L., Brusseau, M.L., Prevatt, F.J., Escobar, B.A., 2021. Incidence of Pfas in soil following long-term application of class B biosolids. Sci Total Environ 793, 148449. https://doi.org/10.1016/j.scitotenv.2021.148449.

[16] Coffin, E.S., Reeves, D.M., Cassidy, D.P., 2023. PFAS in municipal solid waste landfills: Sources, leachate composition, chemical transformations, and future challenges. Curr Opin Environ Sci Health 31, 100418. https://doi.org/10.1016/j.coesh.2022.100418.

[17] D’Ambro, E.L., Pye, H.O.T., Bash, J.O., Bowyer, J., Allen, C., Efstathiou, C., Gilliam, R.C., Reynolds, L., Talgo, K., Murphy, B.N., 2021. Characterizing the Air Emissions, Transport, and Deposition of Per- and Polyfluoroalkyl Substances from a Fluoropolymer Manufacturing Facility. Environ Sci Technol 55 (2), 862–870. https://doi.org/10.1021/acs.est.0c06580.

[18] McGarr, J.T., Mbonimpa, E.G., McAvoy, D.C., Soltanian, M.R., 2023. Fate and Transport of Per- and Polyfluoroalkyl Substances (PFAS) at Aqueous Film Forming Foam (AFFF) Discharge Sites: A Review. Soil Syst 7 (2). https://doi.org/10.3390/soilsystems7020053.

[19] Reinikainen, J., Perkola, N., Äystö, L., Sorvari, J., 2022. The occurrence, distribution, and risks of PFAS at AFFF-impacted sites in Finland. Sci Total Environ 829, 154237. https://doi.org/10.1016/j.scitotenv.2022.154237.

[20] Kim, H., Ekpe, O.D., Lee, J.-H., Kim, D.-H., Oh, J.-E., 2019. Field-scale evaluation of the uptake of Perfluoroalkyl substances from soil by rice in paddy fields in South Korea. Sci Total Environ 671, 714–721. https://doi.org/10.1016/j.scitotenv.2019.03.240.

[21] Wang, P., Wang, T., Giesy, J.P., Lu, Y., 2013. Perfluorinated compounds in soils from Liaodong Bay with concentrated fluorine industry parks in China. Chemosphere 91 (6), 751–757. https://doi.org/10.1016/j.chemosphere.2013.02.017.

[22] Zhu, H., Kannan, K., 2019. Distribution and partitioning of perfluoroalkyl carboxylic acids in surface soil, plants, and earthworms at a contaminated site. Sci Total Environ 647, 954–961. https://doi.org/10.1016/j.scitotenv.2018.08.051.

[23] Brusseau, M.L., Anderson, R.H., Guo, B., 2020. PFAS concentrations in soils: Background levels versus contaminated sites. Sci Total Environ 740, 140017. https://doi.org/10.1016/j.scitotenv.2020.140017.

[24] Dauchy, X., Boiteux, V., Bach, C., Colin, A., Hemard, J., Rosin, C., Munoz, J.-F., 2017. Mass flows and fate of per- and polyfluoroalkyl substances (PFASs) in the wastewater treatment plant of a fluorochemical manufacturing facility. Sci Total Environ 576, 549–558. https://doi.org/10.1016/j.scitotenv.2016.10.130.

[25] Dauchy, X., Boiteux, V., Colin, A., Hémard, J., Bach, C., Rosin, C., Munoz, J.-F., 2019. Deep seepage of per- and polyfluoroalkyl substances through the soil of a firefighter training site and subsequent groundwater contamination. Chemosphere 214, 729–737. https://doi.org/10.1016/j.chemosphere.2018.10.003.

[26] Kucharzyk, K.H., Darlington, R., Benotti, M., Deeb, R., Hawley, E., 2017. Novel treatment technologies for PFAS compounds: A critical review. Glob Trends Environ Remediat Ind 204, 757–764. https://doi.org/10.1016/j.jenvman.2017.08.016.

[27] Schröder, H.Fr, 2003. Determination of fluorinated surfactants and their metabolites in sewage sludge samples by liquid chromatography with mass spectrometry and tandem mass spectrometry after pressurised liquid extraction and separation on fluorine-modified reversed-phase sorbents. 19th Montreux Symp Liq Chromatogr - Mass Spectrom, Supercrit Fluid Chromatogr - Mass Spectrom, Capill Electrophor - Mass Spectrom Tandem Mass Spectrom 1020 (1), 131–151. https://doi.org/10.1016/S0021-9673(03)00936-1.

[28] Cardoso, I.M.F., Pinto da Silva, L., Esteves da Silva, J.C.G., 2023. Nanomaterial-Based Advanced Oxidation/Reduction Processes for the Degradation of PFAS. Nanomaterials 13 (10). https://doi.org/10.3390/nano13101668.

[29] Esfahani, E.B., Dixit, F., Zeidabadi, F.A., Johnson, M.R., Mayilswamy, N., Kandasubramanian, B., Mohseni, M., 2023. Ion exchange and advanced oxidation/reduction processes for per- and polyfluoroalkyl substances treatment: A mini-review. Curr Opin Chem Eng 42, 100953. https://doi.org/10.1016/j.coche.2023.100953.

[30] Yao, Y., Sack, T.U., Volchek, K., Brown, C., 2015. PFC-contaminated soil and its remediation strategies: A review. Proc 38th AMOP Tech Semin Environ Contam Response 314–339.

[31] Høisæter, Å., Arp, H.P.H., Slinde, G., Knutsen, H., Hale, S.E., Breedveld, G.D., Hansen, M.C., 2021. Excavated vs novel in situ soil washing as a remediation strategy for sandy soils impacted with per- and polyfluoroalkyl substances from aqueous film forming foams. Sci Total Environ 794, 148763. https://doi.org/10.1016/j.scitotenv.2021.148763.

[32] Quinnan, J., Morrell, C., Nagle, N., Maynard, K.G., 2022. Ex situ soil washing to remove PFAS adsorbed to soils from source zones. Remediat J 32 (3), 151–166. https://doi.org/10.1002/rem.21727.

[33] Ross, I., McDonough, J., Miles, J., Storch, P., Thelakkat Kochunarayanan, P., Kalve, E., Hurst, J., S. Dasgupta, S., Burdick, J., 2018. A review of emerging technologies for remediation of PFASs. Remediat J 28 (2), 101–126. https://doi.org/10.1002/rem.21553.

[34] Travar, I., Uwayezu, J.N., Kumpiene, J., Yeung, L.W.Y., 2021. Challenges in the PFAS Remediation of Soil and Landfill Leachate: A Review. Adv Environ Eng Res 02 (02), 006. https://doi.org/10.21926/aeer.2102006.

[35] Senevirathna, S.T.M.L.D., Mahinroosta, R., Li, M., KrishnaPillai, K., 2021. In situ soil flushing to remediate confined soil contaminated with PFOS- an innovative solution for emerging environmental issue. Chemosphere 262, 127606. https://doi.org/10.1016/j.chemosphere.2020.127606.

[36] Robert, T., Martel, R., Conrad, S.H., Lefebvre, R., Gabriel, U., 2006. Visualization of TCE recovery mechanisms using surfactant–polymer solutions in a two-dimensional heterogeneous sand model. J Contam Hydrol 86 (1), 3–31. https://doi.org/10.1016/j.jconhyd.2006.02.013.

[37] Rao, P.S.C., Annable, M.D., Sillan, R.K., Dai, D., Hatfield, K., Graham, W.D., Wood, A.L., Enfield, C.G., 1997. Field-scale evaluation of in situ cosolvent flushing for enhanced aquifer remediation. Water Resour Res 33 (12), 2673–2686. https://doi.org/10.1029/97WR02145.

[38] Hayden, N.J., Van der Hoven, E.J., 1996. Alcohol flushing for enhanced removal of coal tar from contaminated soils. Water Environ Res 68 (7), 1165–1171. https://doi.org/10.2175/106143096X128595.

[39] Jawitz, J.W., Annable, M.D., Rao, P.S.C., Rhue, R.D., 1998. Field Implementation of a Winsor Type I Surfactant/Alcohol Mixture for in Situ Solubilization of a Complex LNAPL as a Single-Phase Microemulsion. Environ Sci Technol 32 (4), 523–530. https://doi.org/10.1021/es970507i.

[40] Chen, W., Zhang, X., Mamadiev, M., Wang, Z., 2017. Sorption of perfluorooctane sulfonate and perfluorooctanoate on polyacrylonitrile fiber-derived activated carbon fibers: In comparison with activated carbon. RSC Adv 7 (2), 927–938. https://doi.org/10.1039/C6RA25230C.

[41] Du, Z., Deng, S., Liu, D., Yao, X., Wang, Y., Lu, X., Wang, B., Huang, J., Wang, Y., Xing, B., Yu, G., 2016. Efficient adsorption of PFOS and F53B from chrome plating wastewater and their subsequent degradation in the regeneration process. Chem Eng J 290, 405–413. https://doi.org/10.1016/j.cej.2016.01.077.

[42] Zaggia, A., Conte, L., Falletti, L., Fant, M., Chiorboli, A., 2016. Use of strong anion exchange resins for the removal of perfluoroalkylated substances from contaminated drinking water in batch and continuous pilot plants. Water Res 91, 137–146. https://doi.org/10.1016/j.watres.2015.12.039.

[43] Deng, S., Nie, Y., Du, Z., Huang, Q., Meng, P., Wang, B., Huang, J., Yu, G., 2015. Enhanced adsorption of perfluorooctane sulfonate and perfluorooctanoate by bamboo-derived granular activated carbon. J Hazard Mater 282, 150–157. https://doi.org/10.1016/j.jhazmat.2014.03.045.

[44] Punyapalakul, P., Suksomboon, K., Prarat, P., Khaodhiar, S., 2013. Effects of Surface Functional Groups and Porous Structures on Adsorption and Recovery of Perfluorinated Compounds by Inorganic Porous Silicas. Sep Sci Technol 48 (5), 775–788. https://doi.org/10.1080/01496395.2012.710888.

[45] Zhao, D., Li, H.-B., Xu, J.-Y., Luo, J., Ma, L.Q., 2015. Arsenic extraction and speciation in plants: Method comparison and development. Sci Total Environ 523, 138–145. https://doi.org/10.1016/j.scitotenv.2015.03.051.

[46] Siriwardena, D.P., James, R., Dasu, K., Thorn, J., Iery, R.D., Pala, F., Schumitz, D., Eastwood, S., Burkitt, N., 2021. Regeneration of per- and polyfluoroalkyl substance-laden granular activated carbon using a solvent based technology. J Environ Manag 289, 112439. https://doi.org/10.1016/j.jenvman.2021.112439.

[47] Shaikh, M.A.N., Sarkar, P., Nawaz, T., 2023. PFOA remediation from aqueous media using CTAB impregnated activated carbon: A closed-loop sustainable study with comprehensive selectivity analysis. J Water Process Eng 54, 103965. https://doi.org/10.1016/j.jwpe.2023.103965.

[48] Omirbekov, S., Colombano, S., Alamooti, A., Batikh, A., Cochennec, M., Amanbek, Y., Ahmadi-Senichault, A., Davarzani, H., 2023. Experimental study of DNAPL displacement by a new densified polymer solution and upscaling problems of aqueous polymer flow in porous media. J Contam Hydrol 252, 104120. https://doi.org/10.1016/j.jconhyd.2022.104120.

[49] Rodríguez de Castro, A., Ben Abdelwahed, A., Bertin, H., 2023. Enhancing pollutant removal from contaminated soils using yield stress fluids as selective blocking agents. J Contam Hydrol 255, 104142. https://doi.org/10.1016/j.jconhyd.2023.104142.

[50] Omirbekov, S., Davarzani, H., Ahmadi-Senichault, A., 2020. Experimental Study of Non-Newtonian Behavior of Foam Flow in Highly Permeable Porous Media. Ind Eng Chem Res 59 (27), 12568–12579. https://doi.org/10.1021/acs.iecr.0c00879.

[51] Zhao, Y.S., Su, Y., Lian, J.R., Wang, H.F., Li, L.L., Qin, C.Y., 2016. Insights on Flow Behavior of Foam in Unsaturated Porous Media during Soil Flushing. Water Environ Res 88 (11), 2132–2141. https://doi.org/10.2175/106143016X14733681695483.

[52] Martel, K.E., Martel, R., Lefebvre, R., Gélinas, P.J., 1998. Laboratory Study of Polymer Solutions Used for Mobility Control During In Situ NAPL Recovery. Groundw Monit Remediat 18 (3), 103–113. https://doi.org/10.1111/j.1745-6592.1998.tb00734.x.

[53] Gauthier, M., Kueper, B.H., 2006. Removal of PCB-DNAPL from a rough-walled fracture using alcohol/polymer flooding. J Contam Hydrol 84 (1), 1–20. https://doi.org/10.1016/j.jconhyd.2005.10.012.

[54] Silva, J.A.K., Liberatore, M., McCray, J.E., 2013. Characterization of Bulk Fluid and Transport Properties for Simulating Polymer-Improved Aquifer Remediation. J Environ Eng 139 (2), 149–159. https://doi.org/10.1061/(ASCE)EE.1943-7870.0000616.

[55] Li, H., Dong, Q., Zhang, M., Gong, T., Zan, R., Wang, W., 2023. Transport behavior difference and transport model of long- and short-chain per- and polyfluoroalkyl substances in underground environmental media: A review. Environ Pollut 327, 121579. https://doi.org/10.1016/j.envpol.2023.121579.

[56] Sima, M.W., Jaffé, P.R., 2021. A critical review of modeling Poly- and Perfluoroalkyl Substances (PFAS) in the soil-water environment. Sci Total Environ 757, 143793. https://doi.org/10.1016/j.scitotenv.2020.143793.

[57] Brusseau, M.L., 2020. Simulating PFAS transport influenced by rate-limited multi-process retention. Water Res 168, 115179. https://doi.org/10.1016/j.watres.2019.115179.

[58] Brusseau, M.L., Yan, N., Glubt, S.V., Wang, Y., Chen, W., Lyu, Y., Dungan, B., Carroll, K.C., Holguin, F.O., 2019. Comprehensive retention model for PFAS transport in subsurface systems. Water Res 148, 41–50. https://doi.org/10.1016/j.watres.2018.10.035.

[59] Qi, L., Li, R., Wu, Y., Lin, X., Chen, G., 2022. Effect of solution chemistry on the transport of short-chain and long-chain perfluoroalkyl carboxylic acids (PFCAs) in saturated porous media. Chemosphere 303, 135160. https://doi.org/10.1016/j.chemosphere.2022.135160.

[60] Umeh, A.C., Naidu, R., Olisa, E., Liu, Y., Qi, F., Bekele, D., 2024. A systematic investigation of single solute, binary and ternary PFAS transport in water-saturated soil using batch and 1-dimensional column studies: Focus on mixture effects. J Hazard Mater 461, 132688. https://doi.org/10.1016/j.jhazmat.2023.132688.

[61] Xing, Y., Li, Q., Chen, X., Fu, X., Ji, L., Wang, J., Li, T., Zhang, Q., 2021. Different transport behaviors and mechanisms of perfluorooctanoate (PFOA) and perfluorooctane sulfonate (PFOS) in saturated porous media. J Hazard Mater 402, 123435. https://doi.org/10.1016/j.jhazmat.2020.123435.

[62] Brusseau, M.L., Khan, N., Wang, Y., Yan, N., Van Glubt, S., Carroll, K.C., 2019. Nonideal Transport and Extended Elution Tailing of PFOS in Soil. Environ Sci Technol 53 (18), 10654–10664. https://doi.org/10.1021/acs.est.9b02343.

[63] Zhou, D., Brusseau, M.L., Zhang, Y., Li, S., Wei, W., Sun, H., Zheng, C., 2021. Simulating PFAS adsorption kinetics, adsorption isotherms, and nonideal transport in saturated soil with tempered one-sided stable density (TOSD) based models. J Hazard Mater 411, 125169. https://doi.org/10.1016/j.jhazmat.2021.125169.

[64] Brugeron, A., Schomburgk, S., Cabaret, O., Bault, Violaine, Bel, A., Salquèbre, D., & Parmentier, M. (2018). Synthèse sur la cartographie et la caractérisation des alluvions dans le référentiel hydrogéologique BDLISA. Rapport final.

[65] Lavaud, A. (2010). Quantité et composition chimique du carbone dissous (COD) dans les horizons profonds des sols sous prairie ou culture.

[66] Chen, Y.-C., Lo, S.-L., Li, N.-H., Lee, Y.-C., Kuo, J., 2013. Sorption of perfluoroalkyl substances (PFASs) onto wetland soils. Desalin Water Treat 51 (40-42), 7469–7475. https://doi.org/10.1080/19443994.2013.792145.

[67] Bear, J., 1975. Dynamics of Fluids in Porous Media. Soil Sci 120, 162–163.

[68] Tew, K., 2018. Fetter CW, Boving T, Kreamer D (eds): Contaminant Hydrogeology. Environ Earth Sci 77 (22), 745. https://doi.org/10.1007/s12665-018-7921-5.

[69] MURALI, V., Aylmore, G., 1983. Competitive Adsorption During Solute Transport in Soils: 1. Mathematical Models. Soil Sci 135. https://doi.org/10.1097/00010694-198303000-00002.

[70] Milinovic, J., Lacorte, S., Vidal, M., Rigol, A., 2015. Sorption behaviour of perfluoroalkyl substances in soils. Sci Total Environ 511, 63–71. https://doi.org/10.1016/j.scitotenv.2014.12.017.
[71] Mohammad Hanbali, H.H., Hammud, H., 2014. Remediation of lead by pretreated red algae: Adsorption isotherm, kinetic, column modeling and simulation studies. Green Chem Lett Rev 7 (4), 342–358. https://doi.org/10.1080/17518253.2014.955062.
[72] Carreau, P.J., 1972. Rheological Equations from Molecular Network Theories. Trans Soc Rheol 16 (1), 99–127. https://doi.org/10.1122/1.549276.
[73] Jang, H.Y., Zhang, K., Chon, B.H., Choi, H.J., 2015. Enhanced oil recovery performance and viscosity characteristics of polysaccharide xanthan gum solution. J Ind Eng Chem 21, 741–745. https://doi.org/10.1016/j.jiec.2014.04.005.
[74] Xu, L., Xu, G., Liu, T., Chen, Y., Gong, H., 2013. The comparison of rheological properties of aqueous welan gum and xanthan gum solutions. Carbohydr Polym 92 (1), 516–522. https://doi.org/10.1016/j.carbpol.2012.09.082.
[75] Flahive, J.J., Foufopoulos, A., Etzel, M.R., 1994. Alcohol Precipitation of Xanthan Gum from Pure Solutions and Fermentation Broths. Sep Sci Technol 29 (13), 1673–1687. https://doi.org/10.1080/01496399408002164.
[76] Li, F., Fang, X., Zhou, Z., Liao, X., Zou, J., Yuan, B., Sun, W., 2019. Adsorption of perfluorinated acids onto soils: Kinetics, isotherms, and influences of soil properties. Sci Total Environ 649, 504–514. https://doi.org/10.1016/j.scitotenv.2018.08.209.
[77] Nguyen, T.M.H., Bräunig, J., Thompson, K., Thompson, J., Kabiri, S., Navarro, D. A., Kookana, R.S., Grimison, C., Barnes, C.M., Higgins, C.P., McLaughlin, M.J., Mueller, J.F., 2020. Influences of Chemical Properties, Soil Properties, and Solution pH on Soil–Water Partitioning Coefficients of Per- and Polyfluoroalkyl Substances (PFASs). Environ Sci Technol 54 (24), 15883–15892. https://doi.org/10.1021/acs.est.0c05705.
[78] Hubert, M., Arp, H.P.H., Hansen, M.C., Castro, G., Meyn, T., Asimakopoulos, A.G., Hale, S.E., 2023. Influence of grain size, organic carbon and organic matter residue content on the sorption of per- and polyfluoroalkyl substances in aqueous film forming foam contaminated soils—Implications for remediation using soil washing. Sci Total Environ 875, 162668. https://doi.org/10.1016/j.scitotenv.2023.162668.
[79] Oliver, D.P., Li, Y., Orr, R., Nelson, P., Barnes, M., McLaughlin, M.J., Kookana, R. S., 2020. Sorption behaviour of per- and polyfluoroalkyl substances (PFASs) in tropical soils. Environ Pollut 258, 113726. https://doi.org/10.1016/j.envpol.2019.113726.
[80] Ahrens, L., Taniyasu, S., Yeung, L.W.Y., Yamashita, N., Lam, P.K.S., Ebinghaus, R., 2010. Distribution of polyfluoroalkyl compounds in water, suspended particulate matter and sediment from Tokyo Bay, Japan. Chemosphere 79 (3), 266–272. https://doi.org/10.1016/j.chemosphere.2010.01.045.
[81] Dai, Y., Niu, J., Yin, L., Xu, J., Sun, K., 2013. Enhanced sorption of perfluorooctane sulfonate (PFOS) on carbon nanotube-filled electrospun nanofibrous membranes. Chemosphere 93 (8), 1593–1599. https://doi.org/10.1016/j.chemosphere.2013.08.013.
[82] Zareitalabad, P., Siemens, J., Hamer, M., Amelung, W., 2013. Perfluorooctanoic acid (PFOA) and perfluorooctanesulfonic acid (PFOS) in surface waters, sediments, soils and wastewater – A review on concentrations and distribution coefficients. Chemosphere 91 (6), 725–732. https://doi.org/10.1016/j.chemosphere.2013.02.024.
[83] Higgins, C.P., Luthy, R.G., 2006. Sorption of Perfluorinated Surfactants on Sediments. Environ Sci Technol 40 (23), 7251–7256. https://doi.org/10.1021/es061000n.
[84] Vierke, L., Berger, U., Cousins, I.T., 2013. Estimation of the Acid Dissociation Constant of Perfluoroalkyl Carboxylic Acids through an Experimental Investigation of their Water-to-Air Transport. Environ Sci Technol 47 (19), 11032–11039. https://doi.org/10.1021/es402691z.
[85] Cai, W., Navarro, D.A., Du, J., Ying, G., Yang, B., McLaughlin, M.J., Kookana, R. S., 2022. Increasing ionic strength and valency of cations enhance sorption through hydrophobic interactions of PFAS with soil surfaces. Sci Total Environ 817, 152975. https://doi.org/10.1016/j.scitotenv.2022.152975.
[86] Loganathan, N., Wilson, A.K., 2022. Adsorption, Structure, and Dynamics of Short- and Long-Chain PFAS Molecules in Kaolinite: Molecular-Level Insights. Environ Sci Technol 56 (12), 8043–8052. https://doi.org/10.1021/acs.est.2c01054.
[87] Li, C., Zhang, C., Gibbes, B., Wang, T., Lockington, D., 2022. Coupling effects of tide and salting-out on perfluorooctane sulfonate (PFOS) transport and adsorption in a coastal aquifer. Adv Water Resour 166, 104240. https://doi.org/10.1016/j.advwatres.2022.104240.
[88] You, C., Jia, C., Pan, G., 2010. Effect of salinity and sediment characteristics on the sorption and desorption of perfluorooctane sulfonate at sediment-water interface. Environ Pollut 158 (5), 1343–1347. https://doi.org/10.1016/j.envpol.2010.01.009.
[89] Yin, C., Pan, C.-G., Xiao, S.-K., Wu, Q., Tan, H.-M., Yu, K., 2022. Insights into the effects of salinity on the sorption and desorption of legacy and emerging per-and polyfluoroalkyl substances (PFASs) on marine sediments. Environ Pollut 300, 118957. https://doi.org/10.1016/j.envpol.2022.118957.
[90] Zhou, Q., Deng, S., Zhang, Q., Fan, Q., Huang, J., Yu, G., 2010. Sorption of perfluorooctane sulfonate and perfluorooctanoate on activated sludge. Chemosphere 81 (4), 453–458. https://doi.org/10.1016/j.chemosphere.2010.08.009.
[91] Jeon, J., Kannan, K., Lim, B.J., An, K.G., Kim, S.D., 2011. Effects of salinity and organic matter on the partitioning of perfluoroalkyl acid (PFAs) to clay particles. J Environ Monit 13 (6), 1803–1810. https://doi.org/10.1039/C0EM00791A.
[92] Oh, S., Wang, Q., Shin, W.S., Song, D.-I., 2013. Effect of salting out on the desorption-resistance of polycyclic aromatic hydrocarbons (PAHs) in coastal sediment. Chem Eng J 225, 84–92. https://doi.org/10.1016/j.cej.2013.03.069.
[93] OECD. (2002).
[94] Ahrens, L., Bundschuh, M., 2014. Fate and effects of poly- and perfluoroalkyl substances in the aquatic environment: A review. Environ Toxicol Chem 33 (9), 1921–1929. https://doi.org/10.1002/etc.2663.
[95] Endo, S., Matsuzawa, S., 2024. Hydrophobic Sorption Properties of an Extended Series of Anionic Per- and Polyfluoroalkyl Substances Characterized by C18 Chromatographic Retention Measurement. Environ Sci Technol 58 (17), 7628–7635. https://doi.org/10.1021/acs.est.4c02707.
[96] Campos Pereira, H., Ullberg, M., Kleja, D.B., Gustafsson, J.P., Ahrens, L., 2018. Sorption of perfluoroalkyl substances (PFASs) to an organic soil horizon – Effect of cation composition and pH. Chemosphere 207, 183–191. https://doi.org/10.1016/j.chemosphere.2018.05.012.
[97] Lyu, X., Liu, X., Sun, Y., Ji, R., Gao, B., Wu, J., 2019. Transport and retention of perfluorooctanoic acid (PFOA) in natural soils: Importance of soil organic matter and mineral contents, and solution ionic strength. J Contam Hydrol 225, 103477. https://doi.org/10.1016/j.jconhyd.2019.03.009.
[98] Wang, W., Maimaiti, A., Shi, H., Wu, R., Wang, R., Li, Z., Qi, D., Yu, G., Deng, S., 2019. Adsorption behavior and mechanism of emerging perfluoro-2-propoxypropanoic acid (GenX) on activated carbons and resins. Chem Eng J 364, 132–138. https://doi.org/10.1016/j.cej.2019.01.153.
[99] Ahrens, L., Yamashita, N., Yeung, L.W.Y., Taniyasu, S., Horii, Y., Lam, P.K.S., Ebinghaus, R., 2009. Partitioning Behavior of Per- and Polyfluoroalkyl Compounds between Pore Water and Sediment in Two Sediment Cores from Tokyo Bay, Japan. Environ Sci Technol 43 (18), 6969–6975. https://doi.org/10.1021/es901213s.
[100] Zhang, Q., Wu, X., Lyu, X., Gao, B., Wu, J., Sun, Y., 2022. Effects of anionic hydrocarbon surfactant on the transport of perfluorooctanoic acid (PFOA) in natural soils. Environ Sci Pollut Res 29 (17), 24672–24681. https://doi.org/10.1007/s11356-021-17680-3.
[101] Lauwers, A., Vercammen, J., De Vos, D., 2023. Adsorption of PFAS by All-Silica Zeolite β: Insights into the Effect of the Water Matrix, Regeneration of the Material, and Continuous PFAS Adsorption. ACS Appl Mater Interfaces 15 (45), 52612–52621. https://doi.org/10.1021/acsami.3c12321.
[102] Graham, C., Kassar, C., Boyer, T.H., 2024. Alcohol regeneration of anion exchange resin loaded with per- and polyfluoroalkyl substances and organic contaminants. AWWA Water Sci 6 (4), e1380. https://doi.org/10.1002/aws2.1380.
[103] Taylor, T.P., Rathfelder, K.M., Pennell, K.D., Abriola, L.M., 2004. Effects of ethanol addition on micellar solubilization and plume migration during surfactant enhanced recovery of tetrachloroethene. J Contam Hydrol 69 (1), 73–99. https://doi.org/10.1016/S0169-7722(03)00151-7.
[104] Grubb, D.G., Sitar, N., 1999. Mobilization of trichloroethene (TCE) during ethanol flooding in uniform and layered sand packs under confined conditions. Water Resour Res 35 (11), 3275–3289. https://doi.org/10.1029/1999WR900222.
[105] Alamooti, A., Colombano, S., Shoker, A., Ahmadi-Sénichault, A., Lion, F., Cazaux, D., Marion, C., Lagron, J., Sawadogo, I., Davarzani, D., 2024. Enhancing remediation of residual DNAPL in multilayer aquifers: Post-injection of alcohol-surfactant-polymer mixtures. Sci Total Environ 918, 170680. https://doi.org/10.1016/j.scitotenv.2024.170680.
[106] Shook, G.M., Pope, G.A., Kostarelos, K., 1998. Prediction and minimization of vertical migration of DNAPLS using surfactant enhanced aquifer remediation at neutral buoyancy. J Contam Hydrol 34 (4), 363–382. https://doi.org/10.1016/S0169-7722(98)00090-4.
[107] Lewis, A.J., Yun, X., Lewis, M.G., McKenzie, E.R., Spooner, D.E., Kurz, M.J., Suri, R., Sales, C.M., 2023. Impacts of divalent cations (Mg2+ and Ca2+) on PFAS bioaccumulation in freshwater macroinvertebrates representing different foraging modes. Environ Pollut 331, 121938. https://doi.org/10.1016/j.envpol.2023.121938.
[108] Zhao, L., Bian, J., Zhang, Y., Zhu, L., Liu, Z., 2014. Comparison of the sorption behaviors and mechanisms of perfluorosulfonates and perfluorocarboxylic acids on three kinds of clay minerals. Chemosphere 114, 51–58. https://doi.org/10.1016/j.chemosphere.2014.03.098.
[109] Abou-Khalil, C., Kewalramani, J., Zhang, Z., Sarkar, D., Abrams, S., Boufadel, M. C., 2023. Effect of clay content on the mobilization efficiency of per- and polyfluoroalkyl substances (PFAS) from soils by electrokinetics and hydraulic flushing. Environ Pollut 322, 121160. https://doi.org/10.1016/j.envpol.2023.121160.
[110] Navarro, D.A., Oliver, D.P., Simpson, S.L., Kookana, R.S., 2022. Organic carbon and salinity affect desorption of PFAS from estuarine sediments. J Soils Sediment 22 (4), 1302–1314. https://doi.org/10.1007/s11368-022-03172-5.
[111] Cápiro, N., Da Silva, M., Stafford, B., Rixey, W., Alvarez, P., 2008. Microbial response to a release of neat ethanol onto residual hydrocarbons in a pilot-scale aquifer tank. Environ Microbiol 10, 2236–2244. https://doi.org/10.1111/j.1462-2920.2008.01645.x.
[112] Ma, J., Nossa, C.W., Xiu, Z., Rixey, W.G., Alvarez, P.J.J., 2013. Adaptive microbial population shifts in response to a continuous ethanol blend release increases biodegradation potential. Environ Pollut 178, 419–425. https://doi.org/10.1016/j.envpol.2013.03.057.
[113] Xu, Q., Chen, J., Wang, Y., Ke, S., 2022. Quantitative analysis of dominant mechanisms in improving fluid sweeping uniformity in a layered heterogeneous system via xanthan gum addition. Environ Sci Pollut Res 29 (17), 25759–25773. https://doi.org/10.1007/s11356-021-17632-x.

[114] Weng, Z., Yu, J., Deng, Y., Cai, Y., Wang, L., 2023. Mechanical behavior and strengthening mechanism of red clay solidified by xanthan gum biopolymer. *Journal of Central South University*. 1948-1963 30.
[115] Svab, M., Kubal, M., Müllerova, M., Raschman, R., 2009. Soil flushing by surfactant solution: Pilot-scale demonstration of complete technology. J Hazard Mater 163 (1), 410–417. https://doi.org/10.1016/j.jhazmat.2008.06.116.
[116] Yang, Y., Boots, K., Zhang, D., 2012. A Sustainable Ethanol Distillation System. Sustainability 4, 92–105. https://doi.org/10.3390/su4010092.
[117] Selvaraj, M., Banat, F., 2019. Ethanol-Water Separation Using Membrane Technology. In: Bastidas-Oyanedel, J.-R., Schmidt, J.E. (Eds.), Biorefinery: Integrated Sustainable Processes for Biomass Conversion to Biomaterials, Biofuels, and Fertilizers. Springer International Publishing, pp. 211–232. https://doi.org/10.1007/978-3-030-10961-5_9.
[118] de Bruyn, W.J., Clark, C.D., Senstad, M., Toms, N., Harrison, A.W., 2020. Biological degradation of ethanol in Southern California coastal seawater. Mar Chem 218, 103703. https://doi.org/10.1016/j.marchem.2019.103703.
[119] Trang, B., Li, Y., Xue, X.-S., Ateia, M., Houk, K.N., Dichtel, W.R., 2022. Low-temperature mineralization of perfluorocarboxylic acids. Science 377 (6608), 839–845. https://doi.org/10.1126/science.abm8868.
[120] Abu Elella, M.H., Goda, E.S., Gab-Allah, M.A., Hong, S.E., Pandit, B., Lee, S., Gamal, H., Rehman, A. ur, Yoon, K.R., 2021. Xanthan gum-derived materials for applications in environment and eco-friendly materials: A review. J Environ Chem Eng 9 (1), 104702. https://doi.org/10.1016/j.jece.2020.104702.
[121] Chang, I., Im, J., Prasidhi, A.K., Cho, G.-C., 2015. Effects of Xanthan gum biopolymer on soil strengthening. Constr Build Mater 74, 65–72. https://doi.org/10.1016/j.conbuildmat.2014.10.026.
[122] Maire, J., Joubert, A., Kaifas, D., Invernizzi, T., Marduel, J., Colombano, S., Cazaux, D., Marion, C., Klein, P.-Y., Dumestre, A., Fatin-Rouge, N., 2018. Assessment of flushing methods for the removal of heavy chlorinated compounds DNAPL in an alluvial aquifer. Sci Total Environ 612, 1149–1158. https://doi.org/10.1016/j.scitotenv.2017.08.309.